UNIVERSITETET I OSLO
Faculty of Mathematics and Natural Sciences;
Department of Geosciences;
Meteorology and Oceanography Section

FLEXPART validation with the use of CMET balloons

Master thesis in Geosciences

Anniken Celine Mentzoni

1st June 2011

Abstract

During the campaign in August 2010, five controlled meteorological (CMET) balloons where launched from Ny-Ålesund. Paul B. Voss developed the CMET balloons, and they are adapted to operate in the Arctic environment. They are known for their light weight (approximately $\frac{1}{2}$ kg) and the ability to perform repeated vertical soundings. Data from four of the balloons were used. The flight duration ranged between approximately 24 hours to over 3 days, and 9 soundings were performed. The balloon data were compared with the Lagrangian particle dispersion and trajectory model, FLEXPART. FLEXPART is developed by Andreas Stohl. The study shows that the wind speed used by FLEXPART is generally too high and that the relative humidity spanned by the model is generally too narrow. These errors might be originating from the ECMWF data. The potential temperature, on the other hand, is mostly really good. How close resemblance the calculated trajectories from FLEXPART have with the balloons depends on the stability to the modeled air. More sinking air leads to bigger trajectory errors. The calculated average relative horizontal transport deviation (RHTD) for the first 16 hours is constant around 28 %, which are a few percentage points greater than in earlier studies (e.g. Riddle et al. (2006)). This would probably have been more reliable if the ensemble of the trajectories were greater.

Preface

During this thesis I was part of the project "Launch of controlled meteorological balloons from Ny-Ålesund , Research Council of Norway (RCN), Program PolRes, topic NOR-USA (project #196144)". The project was funded by the Research Council of Norway (RCN), and was an extension of the project IPY POLARCAT (International Polar Year). The purpose of this project was to launch a total of (at least) 6 controlled meteorological (CMET) balloons from Ny-Ålesund, during a campaign in August 2010 and in May 2011. All together 10 balloons were launched.

This project was a collaboration between Norwegian and US scientists, namely Paul Bradley Voss (Smith College, US), Andreas Stohl (NILU) and Lars Robert Hole (met.no). Paul Bradley Voss is the designer of the CMET balloons, and he has adapted them to operate in the Arctic environment. The balloons were launched from the German Alfred Wegener Institute for Polar and Marine Research (AWI) and the French Polar Institute Paul Emile Victor (IPEV) (AWIPEV)'s balloon house.

During the campaign in August, Paul Bradley Voss brought two undergrad students with him, namely Helen Gerard Johnston and Elizabeth Farrell Helbling. They could not participate in May, so PostDoc, Tjarda Roberts came instead.

Acknowledgements

First and foremost, I would like to thank my supervisor Lars Robert Hole (at met.no) for excellent guidance throughout this year. Giving me the opportunity to participate in this project and giving me feedback on my thesis. I would also like to thank my co-supervisors Terje Koren Berntsen (at MetOs) and Joseph Henry LaCasce (at MetOs) for answering questions I had and for discussing the results with me.

Thanks to the Research Council of Norway (RCN), without you the project would not have been possible. Thanks to Svalbard Science Forum (SSF)

for financial support (Arctic Field Grant) during the campaign in May.

Alfred Wegener Institute for Polar and Marine Research (AWI) and the French Polar Institute Paul Emile Victor (IPEV) (AWIPEV), thank you so much for letting us borrow your balloon house. The project wouldn't have run so smoothly without it.

I would also like to thank Paul Bradley Voss (at Smith College, US) for teaching me all about the balloons, helping me with the raw data and giving me inspiration. I would also like to thank his students Helen Gerard Johnston and Elizabeth Farrell Helbling for interesting nights in Ny-Ålesund in August; it wouldn't have been as fun without you. A thank to you also, Tjarda Roberts, for your company and the unusual balloon launch. I hope your wrist is perfectly fine again now.

A special thanks to Gunnar Wollan (at MetOs) for setting up FLEXPART, with all its challenges. Thank you for being so patient. Thanks to Sabine Eckhardt (at NILU) for helping me with the initial settings for the model, and Bjørg Rognerud (at MetOs) for finding all the data I needed for it to run.

Tanks to my fellow students for practical help and relaxing lunch breaks.

Finally I want to thank my family and friends, especially my husband Eilert André Mentzoni, for listening to me and supporting me in good and in bad thesis days. Thank you for finding my typos and for putting up with all my thesis talk. Thank you Heidi, that you made me laugh and think about other things when the thesis made my life a mess.

Anniken Celine Mentzoni
May 2011

Figure 1: *Pictures from Ny-Ålesund in August. In the upper right corner from the left: Helen G. Johnston, Lars R. Hole, Paul B. Voss, E. Farrell Helbling and Anniken C. Mentzoni. In the lower left corner from the left: Helen G. Johnston, Paul B. Voss, Lars R. Hole, Anniken C. Mentzoni, E. Farrell Helbling and Terje K. Berntsen.*

Contents

Chapter 1

Introduction

The purpose of this project is to study atmospheric transport processes in the Arctic by the application of Lagrangian controlled meteorological balloons. Balloon trajectories will be compared with theoretical trajectories using the FLEXPART Lagrangian particle dispersion model.

1.1 The climate in Ny-Ålesund

Ny-Ålesund is located on Spitsbergen, the largest island of the Svalbard archipelago, at 78°55' north and 11°56' east. The annual average temperature is -6.3 °C. The coldest month is February, with an average temperature of -14.6 °C. While the warmest month, July, has an average temperature of 4.9 °C [1]. Consequently, it is permafrost in Ny-Ålesund. Still the temperature is relatively mild compared to other places at this latitude. This is due to the remnants of the Gulf Stream that flows northwards up the west coast of Svalbard [2]. Ny-Ålesund is also relatively dry, and the annual rainfall is 355 mm [3]. For comparison, the rainfall rate in Oslo is between 685 mm and 1200 mm [4] and in Bergen between 1815 mm and 3155 mm [5]. There is midnight sun in Ny-Ålesund for four months from April 16 to August 27, and the sun is below the horizon for four months from October 24 to February 18 [6].

The surface winds in Ny-Ålesund are highly affected by the topography of

[1] Meteorologisk institutt [met.no], Normaler for Spitsbergen, `http://retro.met.no/observasjoner/svalbard/normaler_for_kommune_2111.html`. Read 29.09.2010

[2] Kings Bay, Ny-Ålesund, `http://www.kingsbay.no/index.php?option=com_content&view=article&id=70&Itemid=2`. Read 29.09.2010

[3] met.no, Normaler for Spitsbergen, `http://retro.met.no/observasjoner/svalbard/normaler_for_kommune_2111.html`. Read 29.09.2010

[4] met.no, Normaler for Oslo, `http://retro.met.no/observasjoner/oslo/normaler_for_kommune_301.html?kommuner`. Read 29.09.2010

[5] met.no, Normaler for Bergen, `http://retro.met.no/observasjoner/hordaland/normaler_for_kommune_1201.html?kommuner`. Read 29.09.2010

[6] Earth Tools, Sunrise and sunset calendar for 78°55'0.18"N 11°56'0.03"E, `http://www.earthtools.org/suncal.php?lat=78.91671569942953&lng=11.93334106306152`. Read 29.09.2010

Kongsfjorden, which is located south east-north west. The winds tends to follow the fjord, and are relatively unaffected by the large-scale wind direction. The general opinion (not yet been shown as a fact) is that the flow out of the fjord is katabatic, originating from the downwards flow over the glaciers Kongsvegen, Kronebreen and Kongsbreen. Radiative cooling of the surface is necessary to generate katabatic winds, therefore the wind speed is at its maximum during the night (Livik, 2011).

Throughout the campaign 19-26 August 2010 it was midnight sun, so it was never dark. There were clear sky conditions and air temperatures were between -0.9°C and 10.6°C. It became colder during the campaign, and some of the latest days we had a little evening and morning fog, but no rain.

During the campaign, low pressure systems developed over the Atlantic Ocean. These systems then moved over the southern part of Norway and then to Russia. At the same time high pressure systems moved over Greenland as shown in figure 1.1. As the week went by, the atmospheric pressure over Greenland and Svalbard lowered. At the last day of the campaign there were no longer low pressure systems over Norway, and the pressure was about equal to the pressure over Svalbard. The days after the campaign a low pressure system developed over Svalbard and the Barents Sea, as shown in figure 1.2.

1.2 The thesis structure

In this thesis I am going to:
1. Analyze thoroughly datasets from multi-day CMET flights across the North Atlantic / Arctic Ocean.
2. Compare these datasets with trajectory data obtained by the FLEXPART model.

The thesis is organized as follows: Chapter 2 describes some of the background for the thesis. In chapter 3 the theory of the FLEXPART model is described. A presentation of the methods used will be given in chapter 4. This chapter is mainly about the CMET balloons and how they were launched, but the radiosonde balloons, the model settings and how the trajectory errors were calculated are also mentioned. The results will be presented in chapter 5, and in chapter 6 they will be discussed and conclusions will be given. Chapter 7 will describe further work that can be done.

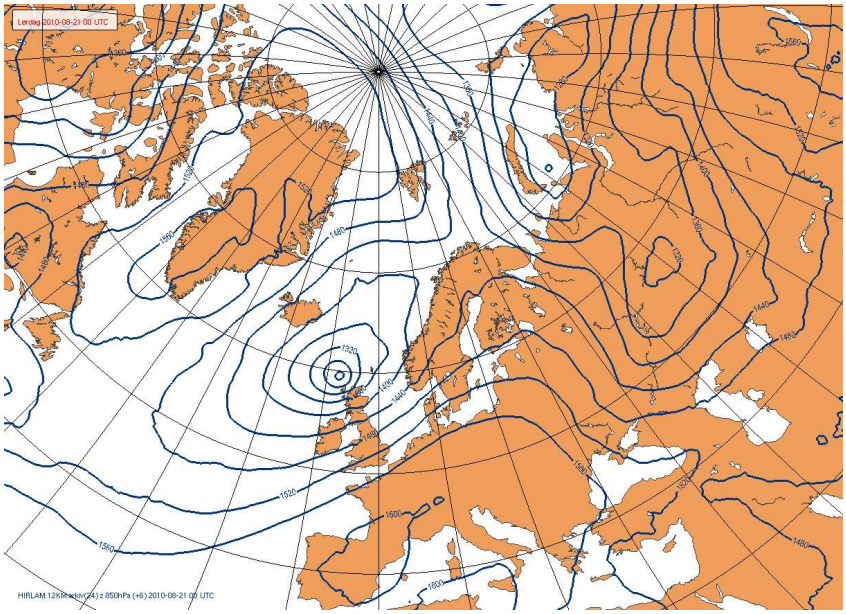

Figure 1.1: *Height of the 850 hPa surface 21 August 2010. The higher the constant pressure surfaces are located, the higher the pressure and temperature are in that area (Holton, 2004).*

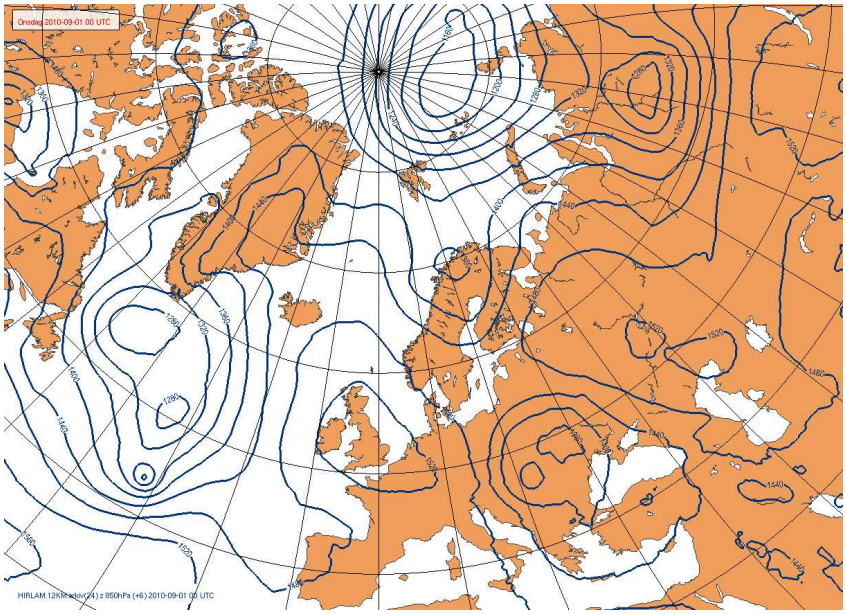

Figure 1.2: *Height of the 850 hPa surface 1 September 2010.*

Chapter 2

Background

Below an overview is given of atmospheric pollution in the Arctic together with examples of applications of free drifting balloons in atmospheric experiments and models used in Arctic research.

2.1 Air pollution

Pollution is an important issue. Each year, more than 2 million people in the world die of air pollution [1]. Increasing population has resulted in more industry, exhaust from cars, agriculture, vegetation fire, aviation and ship traffic. It is well known that this has a great impact on human health [2] and animals life [3], plants [4], and infrastructure (Store norske leksikon, 2010). Most of the pollution comes from highly populated areas, but is transported through the atmosphere and ocean to remote regions. Consequently, pollution also affects the Arctic.

Air pollution produced by industry consists primarily of sulfur dioxide (SO_2), nitrogen oxides (NO_x), particulates, fluorides, nutrients (nitrogen (N) and phosphorus (P)), organic substances or pollutants, heavy metals (lead (Pb), mercury (Hg) and cadmium (Cd)), organic micro-pollutants ($PCBs$ (Polychlorinated biphenyls), $PAHs$ (Polycyclic aromatic hydrocarbons) and other substances) [5] and fluorinated gases [6]. Exhaust from cars consists primarily of SO_2, NO_x, carbon dioxide (CO_2), carbon monoxide (CO), $PAHs$ and

[1] Forente Nasjoner [FN], Atmosfære, `http://www.fn.no/Temaer/Miljoe-og-klima/Miljoe/Atmosfaere`. Read 21.09.2010

[2] World Health Organization [WHO], Air quality and health, `http://www.who.int/mediacentre/factsheets/fs313/en/index.html`. Read 16.09.2010

[3] Miljøstatus i Norge, Lokal luftforurensning, `http://www.miljostatus.no/Tema/Luftforurensning/Lokal-luftforurensning/`. Read 20.09.2010

[4] Ibid.

[5] Norsk institutt for luftforskning [NILU], Industri, `http://www.nilu.no/index.cfm?folder_id=4315&ac=topics`. Read 20.09.2010

[6] Miljøstatus i Norge, Fluorholdige gasser, `http://www.miljostatus.no/Tema/Klima/Klimanorge/Utslipp-avklimagasser/Fluorholdige-gasser-utslipp/`. Read 20.09.2010

Benzene [7]. Pollution from agricultural sources on the other hand, consists primarily of methane (CH_4), nitrous oxide (N_2O) and CO_2 (Hojem and Ohna, 2010). Vegetation fires releases emissions containing mostly CO_2, CO and CH_4 (Langmann et al., 2009). Aviation sources releases mostly CO_2, water vapor, NO_x, SO_2 and soot [8]. Ship traffic releases mostly SO_2 and NO_x [9].

Of these components, CO_2, CH_4, N_2O and fluorinated gases, are the most important anthropogenic greenhouse gases [10]. These gases prevent long-wave (infra-red (IR)) radiation from the earth from emitting into space. This will result in a higher mean temperature in the atmosphere.

Aerosols are small solid, liquid or gas particles, and can affect the radiation balance by absorbing radiation from the sun. One type of aerosol is black carbon (BC), emitted from biomass burning (BB) among others. In the spring there is a lot of BB, because farmers in Eastern Europe burn their fields before they plant new crops. This is done to improve crops, and to reduce insects and diseases. BB is illegal in the Western Europe (Stohl et al., 2007). BC can also be deposited on snow or ice, and hence reduce the surface albedo (Stohl, 2006). This means that the surface will absorb more of the radiation, and reflect less, which again will lead to a higher temperature and accelerate snowmelt (Warneke et al., 2010). Not all aerosols make the temperature rise. Sulfate aerosols, which comes from SO_2, reflect the radiation from the sun, and hence makes it colder [11]. The impact of aerosols depends on what kind of aerosol it is.

2.2 The effect of air pollution on the Arctic

Many scientists have studied the effect of BC, and where the major sources of the BC that reaches the Arctic are. Some of them are Stohl et al. (2007), Shindell et al. (2008) and Warneke et al. (2010).

Shindell et al. (2008) used different models with different physical and chemical aerosol properties, to study O_3 (ozone), CO and BC transport to the Arctic. They found out that deposition of BC outside Greenland is most affected by emissions from Europe throughout the year. Deposition of BC

[7] Folkehelseinstituttet, Avgasser, `http://www.fhi.no/eway/default.aspx?pid=233&trg=MainLeft_5565&MainArea_5661=5565:0:15,3146:1:0:0:::0:0&MainLeft_5565=5544:52281::1:5569:2:::0:0`. Read 20.09.2010

[8] Avinor, Klima: luftfartens klimapåvirkning, `http://www.avinor.no/avinor/miljo/20_Klima`. Read 20.09.2010

[9] Senter for klimaforskning [CICERO], Fritt fram for skipstrafikken?, `http://www.cicero.uio.no/fulltext/index.aspx?id=6368`. Read 20.09.2010

[10] Miljøstatus i Norge, Klimagasser, `http://www.miljostatus.no/Tema/Klima/Klimagasser/`. Read 20.09.2010

[11] NILU, Vulkanutbrudd i Karibien forurenser atmosfæren, `http://www.nilu.com/index.cfm?ac=news&folder_id=4316&text_id=20691&view=text`. Read 05.10.2010

on Greenland on the other hand, is mostly affected by emissions from North America through every season except winter, when emissions from North America and Europe affect the BC just as much. Shindell et al. (2008) also concluded that the Arctic surface concentrations of BC are most sensitive to the European emissions in the winter, and most sensitive to Asian emissions in the spring. In the middle troposphere (500 hPa), the sensitivity is mostly affected by European emissions in the summer, and by Asian emissions in the spring (Shindell et al., 2008).

Warneke et al. (2010) used aircrafts, pictures from the MODIS instruments on satellites and the FLEXPART model (see section 2.5) to study how the spring fires in Russia 2008 led to more BC in the Arctic. They found that the fires resulted in more than doubling (150% increase) of the atmospheric background, also called Artic Haze. This is much more than aerosol sulfate (30% increase), and that is because the background consists of more sulfate than BC (Warneke et al., 2010).

Koch and Hansen (2005) suggest that Europe and south Asia have the same contribution to the BC concentration in the lower Arctic atmosphere, and that south Asia is the main source when looking at the whole column (Stohl, 2006).

In the Arctic a higher temperature, due to BC and other aerosols, will make the sea ice and glaciers melt. This results in smaller habitats for animals like polar bears, seals and seabirds [12]. Increases in temperature can also get the permafrost to thaw. This can lead to flooding and landslides, which again can destroy infrastructure [13]. Less sea ice makes ship trafficking easier (the north-west passage and the northern sea route), and this will increase the emissions of fossil fuel and the risk of oil spills in the Arctic [14]. Pollution can also lead to toxic deposition of PCB, and heavy metals, like Hg, that the animals can ingest. Animals that are on top of the food chain will be most exposed to these pollutants. For example polar bears [15], polar foxes and polar gulls [16]. PCBs degrade slowly and can dissolve in fat tissue. The consequence of this, is that the PCB can follow the generations through eggs, through the uterus to the fetus and through breastfeeding [17].

[12]CICERO, Faktaark 2, http://acia.cicero.uio.no/acia_faktaark_2_krise_for_dyr_paa_isen.html. Read 15.09.2010

[13]CICERO, Faktaark 5, http://acia.cicero.uio.no/acia_faktaark_5_klimaendringer_paavirker_bygninger_farbarhet.html. Read 15.09.2010

[14]CICERO, Faktaark 6, http://acia.cicero.uio.no/acia_faktaark_6_okt_temperatur_nye_muligheter.html. Read 15.09.2010

[15]Norsk Polarinstitutt [NP], Faktaark: arktis-isbjørn, http://npweb.npolar.no/Artikler/2008/1208944774.44. Read 15.09.2010

[16]Miljøstatus i Norge, PCB, http://www.miljostatus.no/Tema/Kjemikalier/Noen-farlige-kjemikalier/PCB/. Read 02.11.2010

[17]Ibid.

Acidification is also a problem in the Arctic, primarily because of anthropogenic emissions of S (sulfur) and N, because of the sensitive ecology and because the levels of acid deposition exceed the system's acid neutralizing capacity (Hole et al., 2009).

Hole et al. (2009) studied the trends in the Arctic acidification from late 70s until 2008. They also compared data from 1991-2004 with the Danish Eulerian Hemispheric Model (DEHM) (see section 2.5), and used DEHM to look at the concentrations of SO_x (oxidized sulfur) and NO_x in air and depositions from the late 1800 to 2020. They found out that SO_4^{2-} (sulfate) concentrations are reduced, mainly because of reduction of emissions in Europe and the Northern America, and that the air and precipitation patterns of NO_3^- (nitrate) and NH_4^+ (ammonium) concentrations are unclear. It is also difficult to project the future emissions and depositions patterns in the Arctic, because of change of climate, increased human activities and new emission control technologies. Their results seem to rule out South East Asia as major source of pollution in the Arctic (Hole et al., 2009).

Chemical compounds, like SO_2 and NO_x, have a tendency to break down more slowly in cold than in warm climates (Hole et al., 2009). The aerosol lifetime is also longer in the Arctic (especially in the winter), because of the extreme dryness in the Arctic troposphere which minimize wet deposition. Dry deposition is also reduced in the Arctic winter time, because of the thermally stable stratification caused by very low temperatures. The stratification causes surface-based inversions that reduce turbulent mixing (Stohl, 2006; Stohl et al., 2007).This often leads to Arctic Haze, which mainly is a consequence of long range transported air pollutants (Hole et al., 2009) and the long aerosol life time. This makes the Haze most prominent in the winter and early spring (Stohl, 2006).

2.3 Transport of air pollution

The Arctic lower troposphere is isolated from the rest of the atmosphere by the Arctic front. The front is formed by constant potential temperature surfaces over the Arctic, with minimum values in the boundary layer. It works as a transport barrier for pollution. In order to penetrate this barrier, the region of the pollution source must have the same low potential temperature as the Arctic (Stohl, 2006). The life time of the pollutants must also be longer than the transport time.

It is important to understand where the pollution is transported from, in order to find a way to reduce the emissions where they occur. Stohl (2006) found that there were several pathways for the transport, and that it was easier for the polluted air parcels to penetrate the Arctic front in the winter.

This is because the snow covered land in the winter makes it possible for the air parcels that pass by, to be cool enough to penetrate the front.

Stohl also looked at transport from the stratosphere, and found out that this transport had marginal significance near the Arctic surface. The reason for this, is that there is negligible stratospheric transport in summer, and in winter the stratospheric air will follow the isentropic surfaces at the Arctic front, and end up in the middle latitudes, before it enter the Arctic. The stratospheric air will be well mixed when it eventually reaches the Arctic lower troposphere, and it will have lost its stratospheric character.

By looking at trajectories from major pollution sources into the Arctic, Stohl found three main pathways. (1) Rapid (4 days or less) low-level transport from densely populated regions in Europe (because Europe is the only continent that can have major emission regions located north of the Arctic front). This is also the most common transport route from boreal forest fires into the Arctic. (2) Low-level transport (10-15 days) over snow covered land from Europe and northern part of Asia (exists only in the winter). Because of the flow's low moisture content and stable stratification, this pathway can transport highly polluted air into the Arctic. (3) Ascent from pollution sources in North America and East Asia (less frequent in Europe), resulting in a slow descent into the Arctic due to radiational cooling. For this transport route, wet scavenging outside the Arctic is likely very efficient (Stohl, 2006).

2.4 Applications of drifting balloons to study the atmospheric boundary layer

The use of balloons is one means of quantifying transport in the atmosphere. Other tools that have also been used are modeling (se section 2.5), satellite images and tracers. Over the years, the balloons size and shape have changed and the content of the payload has increased.

2.4.1 Tetroon balloons

Historically, constant volume balloons (CVB) have been the most commonly used balloons for air mass tracking (Riddle et al., 2006). Bretherton and Pincus (1995) used constant-volume Tetroon balloons in 1992 on the Atlantic Stratocumulus Transition Experiment (ASTEX) to study the marine boundary layer (MBL). The balloons were ballasted to rise 500-750 m above sea level, and they were equipped with GPS (Global Positioning System) receiver that determined the balloons position every five minutes, and transmitted its data to the closest airplane (Bretherton and Pincus, 1995). The Tetroon balloons were maid of Mylar, and had a tetrahedral shape (Businger and Johnson, 2000).

The balloon that survived through the entire last part of the campaign was used to determine the air mass trajectory. Together with flight, satellite and ship observations, and MBL models, they became closer to understand the evolution of a moving marine air mass and its cloud cover, and the physics that interact to determine the structure and cloud cover of the MBL (Bretherton and Pincus, 1995).

2.4.2 Smart balloons

Through the ACE 1 campaign in 1995, Businger et al. (1999) used improved Tetroon balloons, called Smart balloons or Smart Tetroons. They differ from the Tetroons by having a pump and a valve, which makes it possible to automatically adjust the buoyancy, when the balloon travels vertically outside a range of pressure set prior to the release. With the improved version it was also possible to measure temperature, pressure, relatively humidity and balloon status, in addition to GPS signals, which was sent to the aircraft. They released the balloons from a ship south of Tasmania in Australia, to monitor changes in the sulfur budget in the MBL (Businger et al., 1999)

2.4.3 Controlled meteorological balloons

Controlled meteorological (CMET) balloons have been used previously by Riddle et al. (2006) in the ICARTT campaign in 2004, and by Voss et al. (2010) in the MILARGO campaign in 2006. CMET balloons are different from Tetroons and Smart balloons, because the outer balloon envelope is constructed out of flexible material. This makes it possible for the balloon volume to change with height. The disadvantage is that this decreases its natural stability to stay floating at a constant altitude. To compensate for its instability, the CMET balloon has to have an active buoyancy control algorithm. With the CMET balloons, it is also possible to perform repeated soundings during transport, which was not possible with the Smart balloons.

Riddle et al. (2006) used both Smart balloons and CMET balloons to study the transport and chemical transformation of pollutants in the eastern United States and Canada. The CMET balloons payload consisted of a GPS receiver, a two-way satellite modem, a temperature sensor, a pressure transducer and, for one flight, relative humidity and ozone instrument (Riddle et al., 2006).

The goal of the MILARGO campaign was to study the impacts of downstream pollution from the megacity[18] Mexico City. Voss et al. (2010) performed repeated soundings to see the evolving vertical structure of the atmosphere. The payload consisted of a temperature and a humidity sensor, a satellite modem, a GPS receiver and solar panels coupled with a lithium battery. They found that the plume from the city could retain its identity for at least 24-30 h, at the highest altitude, and likely much longer (Voss et al., 2010).

[18]A city consisting of more than 10 million inhabitants.

2.5 Modeling atmospheric chemistry in the Arctic

2.5.1 Danish Eulerian Hemispheric Model

There are several models which have been used in the modeling of atmospheric chemistry in the Arctic. One of them is the Danish Eulerian Hemispheric Model (DEHM) (Christensen, 1997), which is a 3-D atmospheric transport model. The DEHM is really a part of the Danish Eulerian Hemispheric Model system, which also consist of a weather forecast model and the PSU/NCAR Mesoscale Model version 5 (MM5).

There are different versions of the model. The original version has been used since 1991, and the original purpose of developing the model was to study long-range transport of SO_2, SO_4^{2-} and Pb into the Arctic. Another version includes an extensive chemistry scheme, which makes it possible to calculate concentrations and depositions of various pollutants in addition to transport and exchange of atmospheric CO_2.

Hole et al. (2009) used this model, with the extensive chemistry scheme, to calculate trends of the Arctic acidification due to anthropogenic sources of SO_x and NO_x from the late 70s to recent years. Then they compared the result with observation data from the period 1991-2004. They also used DEHM to calculate the total SO_x and NO_x concentrations from the late 1800s to 2020 (Hole et al., 2009).

2.5.2 Weather Research and Forecasting model

Another model used is the Weather Research and Forecasting (WRF) model, which predicts the weather. The WRF model can also include different schemes, which makes it possible to predict more than the weather, for example a chemistry scheme (WRF/Chem). With this scheme it is possible to describe how emissions are exposed to chemical reactions, transport, dry and wet deposition.

Mölders et al. (2010) used the WRF/Chem model to study the effect of the emissions from fishing boats, cargo ships and tourist cruise-ships during the summer in Alaska. They found out that topography had much to do with the pollutants (NO_x, SO_2, O_3, PAN (peroxyacetyl nitrate), HNO_3 (nitric acid) and $PM_{2.5}$ (particulate matter)) impact on the air quality (Mölders et al., 2010).

2.5.3 FLEXPART

A third model which has been used several times in the research of the atmosphere in the Arctic is the FLEXPART Lagrangian particle dispersion model,

originally written by Andreas Stohl. This model has been used by several scientists, mostly to study the transport of pollution into the Arctic (Stohl et al., 2007; Stohl, 2006). (It has also been used in other parts of the world and in combination with other models, for example in Mexico with the MM5 and the WRF model (Voss et al., 2010)).

ICARTT campaign
Riddle et al. (2006) used the FLEXPART model, among others, in the ICARTT campaign in 2004 (mentioned in the section 2.4). They used the model to plan flight routes and to predict the location of polluted air masses. Their main goal with the campaign was to validate the trajectory models, using the CMET balloons and the aircrafts. They found that the mean relative horizontal transport deviation (RHTD) error for flight segments between 2 and 12 hours measured in percent of the flight distance, was 26% for trajectories based on the 1° (resolution) ECMWF (European Centre for Medium-range Weather Forecast) model, and 34% for trajectories based on the 1° GFS (Global Forecast System) model. This varied little with the resolution. The errors have likely less effect on tracer concentrations than on the cross stream, because the errors where mainly aligned with the flow. Riddle et al. (2006) emphasize that transport due to sub grid scale features, for example a narrow low level jet, may be missed in the models.

Arctic smoke
Stohl et al. (2007) used FLEXPART combined with MODIS instruments on the Aqua and Terra satellites to estimate emissions released by biomass burning (BB), and to see how the smoke was transported. They had observed a lot of pollution on Spitsbergen and Iceland spring 2006, and they wanted to see if there were any connections to the agricultural fires in the Eastern Europe. They used both the forward and backward time setting in the model. Forward from the emission field, to see which areas were affected and backward from the Zeppelin station, to look at the potential sources. Stohl et al. (2007) also used the forward setting to see how the CO (carbon monoxide) emissions from fossil fuel combustions (FFC) in Europe, North America and Asia were spreading. They did not take removal processes into account (Stohl et al., 2007).

Stohl et al. (2007) conclude that FFC, compared to BB, had little impact on the CO emissions and aerosol mass, but the NO_x emissions (from FFC) might have had some impact on the O_3 formation. The higher temperature on Spitsbergen also made the transport of the pollutants easier, because the temperature contrast between the Arctic and the midlatitudes was reduced. This makes the transport pattern no 1 (se Section 2.3), rapid low-level transport, more efficient. They also suggest that the observed discolored snow on Spitsbergen came from the dry deposition of smoke aerosols, and that the snow albedo was reduced because of this (Stohl et al., 2007).

Pollution transport
The main pathways for transportation of pollution (described in Section 2.3), are results from using the FLEXPART model. Stohl (2006) used FLEXPART to study the BC emission transport. He did not account for any chemical processes, so the BC is not affected by transformation or any removal mechanisms. Stohl ran the model with 1.4 million imaginary particles, equally distributed in the global atmosphere, for 5 $\frac{1}{2}$ year. Then he found the Arctic particles, which is the particles that stayed for 5 days or more north of 70°N, and used backward in time to find out their possible source (Stohl, 2006). This is how Stohl calculated the 3 main pathways of pollution transport.

The theory of the FLEXPART model will be thoroughly described in chapter 3.

Chapter 3

Theory

FLEXPART is a Lagrangian [1] particle dispersion and trajectory model, which is coded in the Fortran language. A Lagrangian model is easier to use than an Eulerian, because there is no numerical diffusion. The model was originally written by Andreas Stohl under his military service, almost 15 years ago, at the nuclear-biological-chemical school of the Austrian Forces (Stohl et al., 2010). Since then, the model has been updated several times, until the latest version 8.22 [2].

3.1 GRIB files

FLEXPART uses meteorological fields from the European Centre for Medium-range Weather Forecast (ECMWF) numerical prediction model or the National Centers of Environmental Prediction's (NCEP) Global Forecast System (GFS) model. Most used are the ECMWF data. These fields are coded in Gridded Binary (GRIB) format, which makes it possible to store large amount of data in small file sizes (Stohl et al., 2010). The GRIB format is standardized by the World Meteorological Organization (WMO), and consists of data sections divided into octets consisting of 8 bits each. There are two different GRIB files in use, GRIB1 (FM 92-XI) and GRIB2 (World Meteorological Organization, 2010), which has a more flexible and compact format. The newest version of FLEXPART, is now able to read in both GRIB1 and GRIB2 files, and a combination of these (Stohl et al., 2010).

3.2 Input data

Horizontal and vertical wind components, specific humidity and temperature are the three-dimensional fields FLEXPART needs to run. It also needs

[1] Lagrangian means that the model 'follow' the particles, and does not have a fixed coordinate system like an Eulerian model (for example the Danish Eulerian Hemispherical Model (DEHM) used in Hole et al. (2009), see section 2.5).

[2] NILU, FLEXPART, `http://transport.nilu.no/flexpart`. Read 30.05.2011

two-dimensional fields such as surface pressure, 10 m horizontal wind components, 2 m temperature and dew point temperature, total cloud cover, sensible heat flux, east/west and north/south surface stress, large scale and convective precipitation, topography, land-sea-mask and sub grid standard deviation of topography.

The three-dimensional input data is given in η coordinates on the levels of the ECMWF model. They are then converted to terrain following Cartesian coordinates ($\bar{z} = z - z_t$) [3] by the equation:

$$\tilde{w} = \dot{\tilde{z}} = \dot{\tilde{\eta}}(\frac{\partial p}{\partial z})^{-1} + v_h \cdot \nabla_\eta \tilde{z}, \tag{3.1}$$

where $\dot{\tilde{\eta}} = \dot{\eta}\partial p/\partial\eta$. This is done, because parameterized random velocities in the atmospheric boundary layer (ABL) (which is used in the turbulence calculations) is given in terrain following Cartesian coordinates, to reduce time consuming coordinate transformation in every time step (Stohl et al., 2010).

3.3 Calculating the ABL height

The ABL height h_{mix} is calculated using the critical Richardson number concept according to Vogelezang and Holtslag (1996). h_{mix} is the height of the first model level l that has a Richardson number greater than 0.25:

$$Ri_l = \frac{(g/\Theta_{v1})(\Theta_{vl} - \Theta_{v1})(z_l - z_1)}{(u_l - u_1)^2 + (v_l - v_1)^2 + 100u_*^2}. \tag{3.2}$$

Here Θ_{v1} and Θ_{vl} are the virtual potential temperatures. z_1 and z_l are the heights of the 1^{st} and l^{th} model level, respectively. (u_1, v_1) and (u_l, v_l) are the wind components at these levels, and u_* is the friction velocity. If the surface stresses are given from the ECMWF data:

$$u_* = \sqrt{\tau/\rho} \tag{3.3}$$

Here τ is the total surface stress [4] and ρ is the air density. Else u_* must be solved by solving u_*, L and Θ_* iteratively:

$$u_* = \frac{\kappa\Delta u}{ln\frac{z_l}{10} - \Psi_m(\frac{z_l}{L}) + \Psi_m(\frac{10}{L})}, \tag{3.4}$$

[3] z_t is the height of the topography.

[4] $\tau = \sqrt{\tau_1^2 + \tau_2^2}$, where τ_1 and τ_2 are the surface stresses in east/west and north/south direction, respectively.

$$L = \frac{\bar{T}u_*^2}{g\kappa\Theta_*}, \tag{3.5}$$

$$\Theta_* = \frac{\kappa\Delta\Theta}{0.74[ln\frac{z_l}{2} - \Psi_h(\frac{z_l}{L}) + \Psi_h(\frac{2}{L})]}. \tag{3.6}$$

Here κ is the von Kármán constant (0.4), Δu is the difference between wind speed at the second model level and at 10 m, z_l is the height of the second model level, Ψ_m and Ψ_h are the stability correction functions for momentum and heat, respectively. $\bar{T}$ is the average surface layer temperature, g is the acceleration due to gravity, Θ_* is the temperature scale, and $\Delta\Theta$ is the difference between potential temperature at the second model level and at 2 m.

Complex topography, variability in landuse and soil wetness can cause spatial variations of the ABL height. Another problem is when these spatial variations are not resolved by the ECMWF model. To avoid significant bias in the surface tracer concentrations and the tracer cloud thickness, FLEXPART uses an envelope ABL height in the calculations:

$$H_{env} = h_{mix} + min[\sigma_Z, c\frac{V}{N}]. \tag{3.7}$$

Here σ_Z is the standard deviation of the ECMWF model sub grid topography, c is a constant (2.0), V is the wind speed at height h_{mix}, and N is the Brunt-Vaisala frequency. FLEXPART always use the maximum envelope height of the grid points surrounding a particle's position in time and space. Under convective and stable conditions, H_{env} are the ABL height plus the sub grid topography, but under stable conditions the topography is limited by the factor $c\frac{V}{N}$ [5] (Stohl et al., 2010).

3.4 The trajectory equation

To solve the trajectory equation:

$$\frac{d\boldsymbol{X}}{dt} = \boldsymbol{v}[\boldsymbol{X}(t)], \tag{3.8}$$

FLEXPART uses the zero acceleration scheme:

$$\boldsymbol{X}(t + \Delta t) = \boldsymbol{X}(t) + \boldsymbol{v}(\boldsymbol{X}, t)\Delta t, \tag{3.9}$$

[5] $\frac{V}{N}$ is the local Froude number, which is the ratio of inertial to buoyant forces.

where $\boldsymbol{X}$ is the position vector, t is the time, Δt the time increment, and $\boldsymbol{v}$ is the wind vector [6]. This scheme is accurate to the first order. To solve the trajectory equation more accurate, FLEXPART takes one iteration with the second order Petterssen scheme for the grid scale wind, whenever this is possible. It cannot be applied in the ABL if ctl>0 [7], if nested domain is used and a particle crosses the boundary to this domain, and if the winds needed for the second time are outside the memory (Stohl et al., 2010).

3.5 The Langevin equation

The turbulent wind fluctuations $\boldsymbol{v}_t$ can be written as:

$$dv_{t_i} = a_i(\boldsymbol{x}, \boldsymbol{v}_t, t)dt + b_{ij}(\boldsymbol{x}, \boldsymbol{v}_t, t)dW_j, \tag{3.10}$$

when based on the Langevin equation. Here both a and b, the drift term and the diffusion term respectively, are functions of position, turbulent velocity and time. dW_j are incremental components of a Wiener process with mean zero and variance dt. FLEXPART assumes Gaussian turbulence, even when this assumption is violated under convective conditions, because the error this causes is minor when the particles are well mixed in the ABL layer.

Langevin equation for the vertical wind component w can be expressed as:

$$dw = -w\frac{dt}{\tau_{L_w}} + \frac{\partial \sigma_w^2}{\partial z}dt + \frac{\sigma_w^2}{\rho}\frac{\partial \rho}{\partial z}dt + (\frac{2}{\tau_{L_w}})^{1/2}\sigma_w dW. \tag{3.11}$$

Where w are the turbulent vertical wind component, and σ_w its standard deviation. ρ is air density and τ_{L_w} is the Lagrangian timescale for the vertical velocity autocorrelation. The second term on the right hand side is the drift correction, while the third term is the density correction and accounts for the decrease of air density with height. The horizontal wind components can also be written as equation 3.11, but without drift and density correction term. Equation 3.11 can also be written as:

$$d(\frac{w}{\sigma_w}) = -\frac{w}{\sigma_w}\frac{dt}{\tau_{L_w}} + \frac{\partial \sigma_w}{\partial z}dt + \frac{\sigma_w}{\rho}\frac{\partial \rho}{\partial z}dt + (\frac{2}{\tau_{L_w}})^{1/2}dW. \tag{3.12}$$

If the time steps are long, equation 3.11 is used, else equation 3.12 is used (Stohl et al., 2010).

[6] Where $\boldsymbol{v} = \bar{\boldsymbol{v}} + \boldsymbol{v}_t + \boldsymbol{v}_m$, $\bar{\boldsymbol{v}}$ is the grid scale wind, $\boldsymbol{v}_t$ is the turbulent wind fluctuations and $\boldsymbol{v}_m$ is the mesoscale wind fluctuations.

[7] When ctl>0, the time steps are limited by τ_L (the Lagrangian timescale for the velocity autocorrelation). Else FLEXPART uses constant time steps of one synchronization time interval.

3.6 Convective parameterization scheme

The convective parameterization scheme is also called the Emanuel scheme, since it was Emanuel and Živković-Rothman (1999) who wrote it. This scheme is used to compensate for the convective transport that is sub-grid scale in the horizontal direction [8]. This is necessary, because the updrafts and downdrafts in convective clouds are important transport mechanisms, and because horizontal convective transport is not represented by de ECMWF vertical velocity. The scheme prepares a redistribution of particles in the entire vertical column using the provided grid-scale temperature and humidity fields from the original ECMWF model levels (not the Cartesian coordinates). With these fields, the scheme calculates a displacement matrix with the mass flux information needed for the particle redistribution. The matrix is calculated whenever:

$$T_{vp}^{LCL+1} \geq T_{v}^{LCL+1} + T_{thres}, \tag{3.13}$$

where T_{vp}^{LCL+1} is the virtual temperature of a surface air parcel lifted to the level above the LCL [9], T_{v}^{LCL+1} is the virtual temperature of the environment there, and $T_{thres} = 0.9$ K (a threshold temperature value). The matrix calculates the saturated up- and downdrafts, and it is assumed that these fluxes are balanced by a subsidence mass flux in the environment. The actual redistribution of the particles is done in the subroutine redist.f, according to the displacement matrix produced by the convective parameterization scheme. To determine whether, and where, a particle shall be displaced or not, a random number between [0,1] is drawn. Then the compensating subsidence mass fluxes are converted to a vertical velocity, which affects the particles that where not displaced. This conversion is done instead of random displacement, to eliminate numerical diffusion in the cloud-free environment (Stohl et al., 2010).

3.7 Removal processes

FLEXPART can calculate dry and wet deposition, and radioactive decay of tracers, by reducing the particles mass.

3.7.1 Dry deposition

Dry deposition of particulate matter is calculated by the equation:

$$v_d(z) = [r_a(z) + r_b + r_a(z) r_b v_g]^{-1} + v_g. \tag{3.14}$$

[8] The convective transport is grid-scale in the vertical direction.

[9] Lifting condensation level.

Here v_g [10] is the gravitational settling velocity, r_a is the aerodynamic resistance between z and the surface and r_b is the quasilaminar sub layer resistance. Gravitational settling velocity is also important for the particle's trajectory when use of single-species simulations (are switched off in multi species simulations). The velocities are also affected by the particle size, which is why FLEXPART calculate the velocities by using different particle diameters. The particles are assumed to have a logarithmic normal size distribution, and after the velocity calculations the velocities are weighted with their respective particulate mass fractions. The mass loss due to dry deposition is calculated by:

$$\Delta m(t) = m(t)[1 - exp(\frac{-v_d(h_{ref})\Delta t}{2h_{ref}})]. \tag{3.15}$$

This is done for all particles under two times the reference height $2h_{ref}$, and usually h_{ref} is set to 15m (Stohl et al., 2010).

3.7.2 Wet deposition

Wet deposition is calculated if the relative humidity is greater than 80%. FLEXPART then assumes the existence of clouds, and decides whether to calculate in- or below- cloud scavenging. For particles, the in cloud scavenging coefficient Λ follows the scheme of Hertel et al. (1995):

$$\Lambda = \frac{S_i I}{H_i}, \tag{3.16}$$

where I is the precipitation rate, H_i is the height over which scavenging takes place and

$$S_i = 0.9/cl, \tag{3.17}$$

where cl is the cloud liquid content [11].

Below cloud scavenging is described as:

$$m(t + \Delta t) = m(t) \exp(-\Lambda \Delta t), \tag{3.18}$$

where m is the particle mass and

$$\Lambda = AI^B. \tag{3.19}$$

A is the scavenging coefficient at $I = 1$ mm/hour and B gives the dependency on precipitation rate (Stohl et al., 2010).

[10] $v_g = \frac{g\rho_p d_p^2 C_{cun}}{18\mu}$, where d_p is the particle diameter, ρ_p the particle density, μ the dynamic viscosity of air (0.000018 kg $m^{-1}s^{-1}$), and C_{cun} is the Cunningham slip-flow correction.

[11] $cl = 2 * 10^{-7} * I^{0.36}$

3.8 Wesely scheme

There are many different land types on the Earth, depending on roughness, chemical reactivity, etc. IGBP's [12] land cover classification had initially 17 different land use classes, by the help of the Wesely scheme, these 17 classes where transferred into just 13 classes. Each of these classes has a defined roughness length. This roughness length is used to parameterize the surface resistance, which in turn is used to calculate the dry deposition of gases (Stohl et al., 2010).

3.9 Options

There are many options to choose between before running the model. The tracers of choice can be released from a point, line, area or volume sources in the atmosphere. This can easily be programed into the Fortran code, by deciding how many different tracers, which tracers, and their decay time. Other settings that are possible to change are the direction of the simulation and higher resolution in selected areas. The direction can either be forward or backward in time. By choosing the forward in time, it is possible to look at, for example, the dispersion of tracers from their sources, or their trajectories. By choosing the backward in time, it is possible to determine potential source contributions. It is then possible to see trajectories from where the source might be. By choosing to have a nested grid inside the regular grid, it is possible to have better resolution on parts of the area considered. There is also possible to run the model without any removal possesses (Stohl et al., 2010).

[12] International Geosphere-Biosphere Programme.

Chapter 4

Methods

In this chapter the CMET balloons, the balloon launches, the FLEXPART model settings and the trajectory error calculations will be described. Our campaign was from 19-26 August, and we were 3 scientists and 3 students which participated. The professors were Paul B. Voss (who also had to undergrad students with him), Lars R. Hole and Terje K. Berntsen (stayed from 19-23 August).

4.1 Balloon launches

During our campaign we launched 5 CMET balloons, which are the smallest altitude controlled balloons ever launched (Svalbard Science Forum, 2010). They are 80 cm in diameter, 150 cm tall, and weigh approximately 500 g when they are connected to the payload which, weigh 250 g. They were prepared in the Norwegian Polar Institute Sverdrup Research Station, and in the German Alfred Wegener Institute for Polar and Marine Research (AWI) and the French Polar Institute Paul Emile Victor (IPEV) (AWIPEV)'s balloon house in Ny-Ålesund. They were launched from the German and French balloon house, and controlled at the Sverdrup station.

Before the balloons were launched, we used the Air Resources Laboratory (ARL) on National Oceanic and Atmospheric Administration's (NOAA) homepage to compute forecast trajectories. The model is also called Hysplit, and gets its initial values from the GFS model [1]. This was done to see if there were going to be any problems with icing, and to see in which direction the balloons were going to fly (we had to make sure that the balloons did not fly into Russian air space).

4.1.1 Preparation of the balloons

The balloons had been transported as carry-on luggage from the United States, and had to be prepared before we could launch them. The payloads

[1] `http://ready.arl.noaa.gov/HYSPLIT_traj.php`.

consisted of a motherboard connected to sensors that could measure temperature, humidity, pressure, and board status. In addition they had a satellite modem, a GPS receiver, and a solar panel coupled with a lithium battery. The GPS coordinates made it possible to calculate the wind speed and direction from each data point. The balloons had also a pump and a valve that were connected to the payload. The pump and valve assembly controlled the helium flow between the high pressure balloon and the zero pressure balloon. The payload enclosure had also a return address in case someone found them after decent. All the different parts of the payload can be seen in figure 4.1.

Before the balloons were ready to fly, we had to inflate them with helium. We filled the balloons some hours before the launch, to see if there were any leaks. Only the fifth balloon had a small leakage, so we used tape to seal it. When we filled the balloons with helium, we first inflated the high pressure balloon, until the pressure was 20 000 Pa. Then we filled the zero pressure balloon just enough to balance the payload. We also had to talk to the Norwegian aviation authorities (Avinor), before we could launch the balloons. When Avinor was informed, the final helium filling and payload connections were done.

4.1.2 Balloon no 1

The first balloon was launched at midnight the 22th of August (22:02 UTC 21.08.10.). The balloon was terminated after almost 24 hours (22:01 UTC 22.08.10), after receiving a command that led to an open valve. The balloon then rose to 6000 m, before it fell down in the ocean. A bug in the control algorithm was probably also a contributing factor.

4.1.3 Balloon no 2

Balloon no 2 was launched approximately 01:00 the 23th of August (22:55 UTC 22.08.10.). This balloon was terminated after 2 $\frac{1}{2}$ days (15:20 UTC 25.08.10), after having the same bug and receiving the same command as balloon no 1.

4.1.4 Balloon no 3

The third balloon was launched approximately 18:00 the 23th of August (16:27 UTC 23.08.10.). This balloon was terminated just after 3 days in the air (20:10 UTC 26.08.10). The balloon was terminated because it had such a low differential pressure (dp) between the high pressure and zero pressure balloon that it probably would not had survived the night. Balloon no 3 was the balloon that had the longest flight duration.

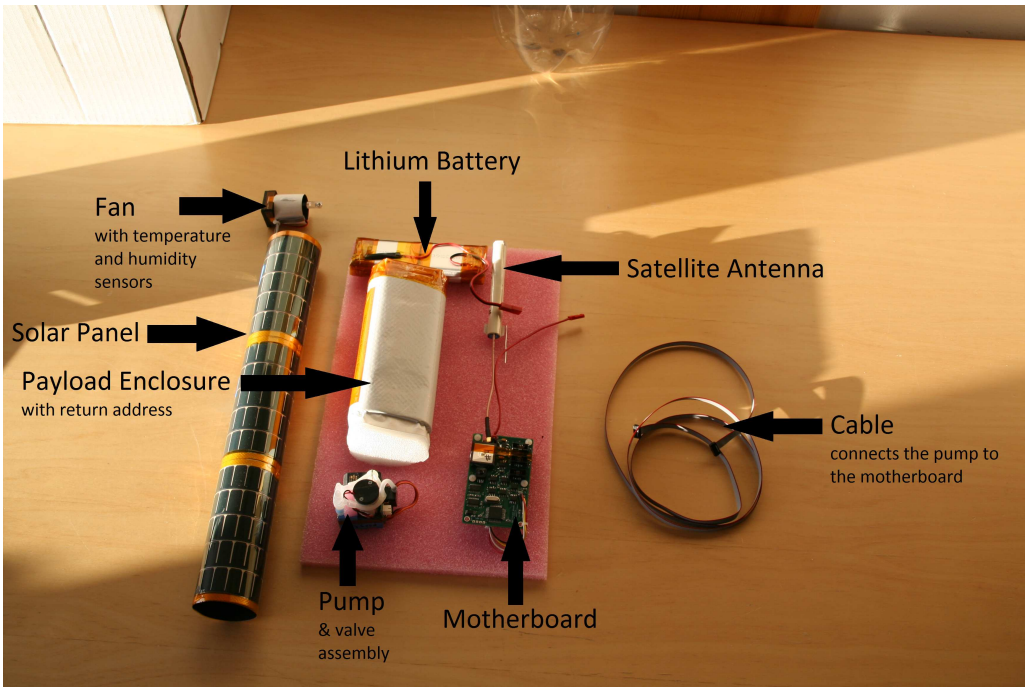

Figure 4.1: *The CMET balloon's payload.*

Figure 4.2: *Shows how the balloons were inflated and then launched. In the pictures in appearing order: Anniken C. Mentzoni, Helen G. Johnston and E. Farrell Helbling*

4.1.5 Balloon no 4

Balloon no 4 was launched approximately 13:00 the 24th of August (10:47 UTC 24.08.10.). The balloon was terminated after almost 2 $\frac{1}{2}$ days (22:00 UTC 26.08.10), because of the same reason as balloon no 3, it had too low dp.

4.1.6 Balloon no 5

The last balloon was launched approximately 04:00 the 25th of August (02 UTC 25.08.10.). This balloon was special, because it was the only balloon with a CO_2 sensor, and was also the balloon with the most technical problems. After we had repaired the leakage, and launched the balloon, we found out that the GPS receiver did not work, so we could not get a correct location of the balloon. After approximately 12 hours we terminated it, because we would not risk that the balloon went in to Russia without us knowing about it. The little data we got from this balloon will not be used.

4.2 Balloon data

Balloon measurements were made every 10 seconds during the ascent, every 10-60 seconds during soundings and every 0.5-3 minutes (up to 10 minutes on balloon no 1) during float. As shown in figure 4.3, the normal float altitude where between 2000-2500 meters. We also preformed repeated vertical soundings on all the balloons except the first one. All together on balloon 2, 3 and 4 we preformed 9 soundings. The balloon trajectories are shown in figure 4.4

4.3 Challenges with launching CMET balloons in the Arctic

There are some challenges with launching CMET balloons in the Arctic. Little sun (except in the summer) and weak sun due to the high latitude makes the battery charging more difficult than on lower latitudes. Since it is so cold in the Arctic, there is also a problem with icing. Ice can accumulate on the balloons' envelope; this can make the balloons to heavy, which will make them decent. There are also complex airspace issues, so even though the CMET balloons are small, launching must be approved by the aviation authorities (Voss et al., 2011).

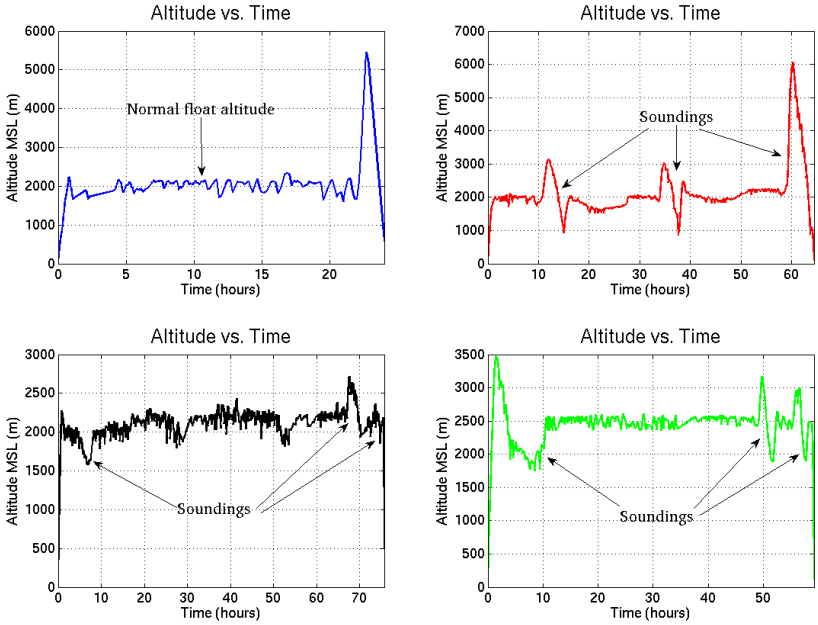

Figure 4.3: *Height vs. time for balloon no 1-4.*

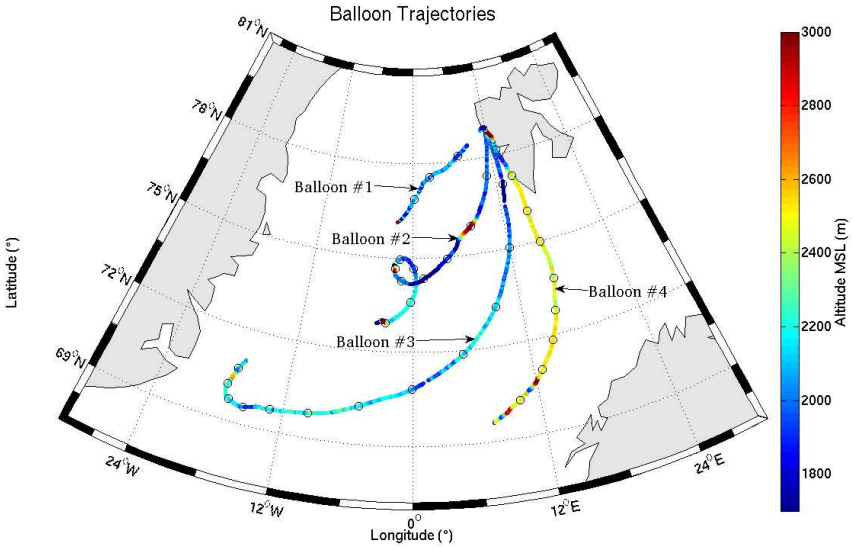

Figure 4.4: *Map of the North Atlantic, showing Svalbard and the CMET balloon trajectories. The balloon altitudes are shown by the colors of the trajectories, while the black circles represent 6-hour intervals.*

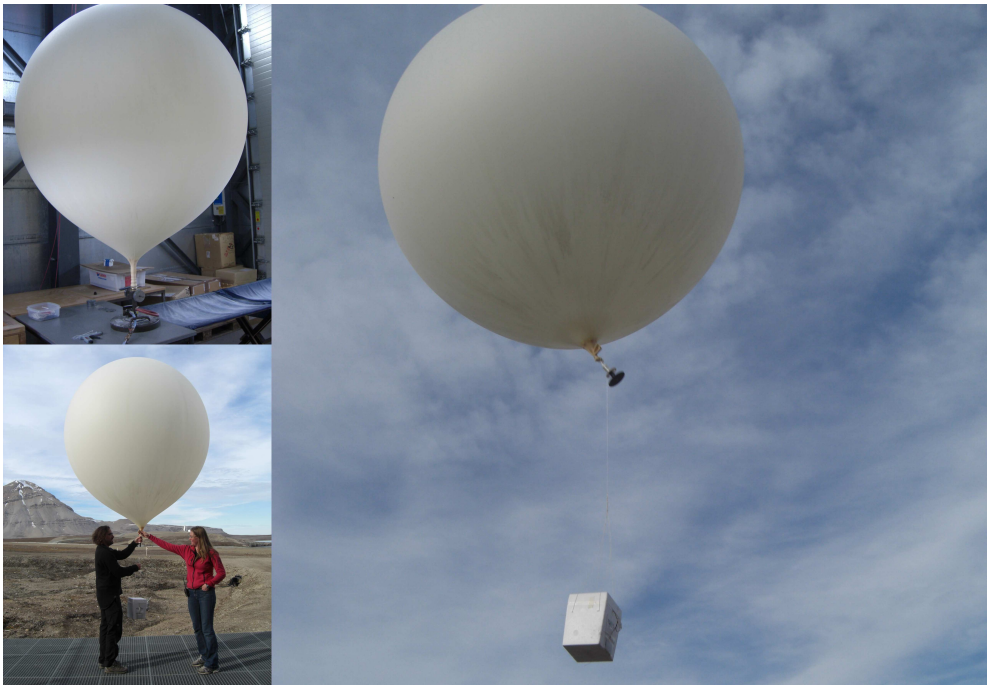

Figure 4.5: *Radiosonde balloon. Inflated with helium and then launched.*

4.4 Radiosonde balloons

Every day during our campaign, the Alfred Wegener Institute launched a radiosonde balloon filled with helium between 11 and 13 o'clock (local time), as shown in figure 4.5. The radiosonde balloons measured pressure, temperature, relative humidity and wind [2]. We used data from the radiosonde balloons and compared it with the CMET balloons ascent.

4.5 Model settings

For this study we used the FLEXPART model [3] with meteorological fields from the ECMWF model with a 0.2° * 0.2° resolution. The fields were given every 3 hours, and the output was calculated for every hour. All removal processes were turned off.

FLEXPART was used to calculate trajectories from the exact time and place of the balloons, and trajectories from a 10 km * 10 km box in the horizontal surrounding the balloons positions, both after the balloons ascent. Trajectories from various heights were also calculated.

[2] Alfred Wegener Institute, Upper Air Soundings at Koldewey, `http://www.awi.de/en/infrastructure/stations/awipev_arctic_research_base/observatories_and_facilities/atmospheric_observatory/meteorological_measurements/upper_air_soundings_at_koldewey/`. Read 10.03.2011.

[3] version 8.0

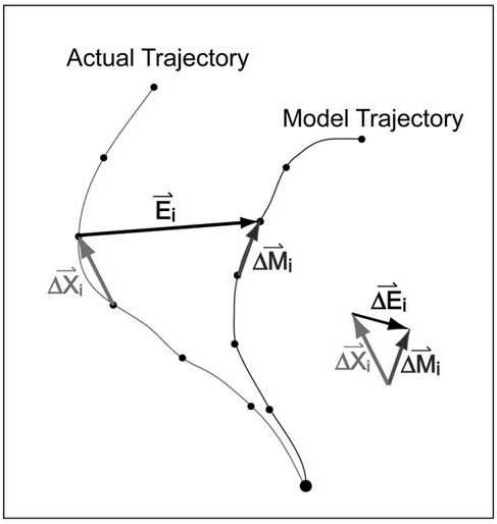

Figure 4.6: *The relationship between the incremental (ΔE_i) and the total (E_i) trajectory errors at a given iteration. E_i is the vector sum of all ΔE_i, and is called the cumulative trajectory error or AHTD (Riddle et al., 2006). The figure is also from Riddle et al. (2006)*

4.6 Trajectory error calculations

We calculated trajectory errors by subtracting the balloon trajectory (the actual trajectory) from the model trajectory for every iteration. ΔE_i represent the incremental position error, and is shown in figure 4.6. The cumulative trajectory error, also known as the absolute horizontal transport deviation (AHTD), is then the vector sum of all the incremental errors. We calculated the relative horizontal transport deviation (RHTD) for every iteration, which is the AHTD divided by the length of the actual trajectory at that time (Riddle et al., 2006).

Chapter 5

Result

5.1 Forecast Trajectories

Figure 5.1-5.4 shows the forecast trajectories for the balloons from NOAA's Hysplit model. The red, blue and green trajectories represent 500 m, 1500 m and 3000 m (2000 m for balloon no 4 in figure 5.4), respectively. The small markers represent 6-hour intervals (placed at 06, 12 and 18 UTC), while the larger ones represent 24-hour intervals stating at midnight (UTC).

As seen from figure 4.4 and the first 24 hours in figure 5.1, the NOAA trajectory is quite similar to the real balloon trajectory. The balloon trajectory is located between the blue and green trajectories, but closer to the blue one.

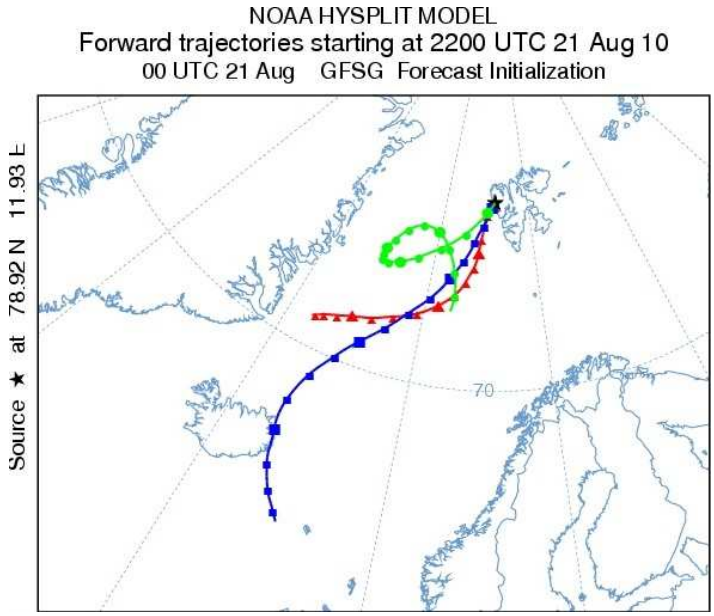

Figure 5.1: *Forecast trajectories for balloon no 1 from NOAA's Hysplit model. Red, blue and green represent 500 m, 1500 m and 3000 m, respectively. The small markers represent 6-hour intervals (placed at 06, 12 and 18 UTC), while the larger ones represent 24-hour intervals stating at midnight (UTC).*

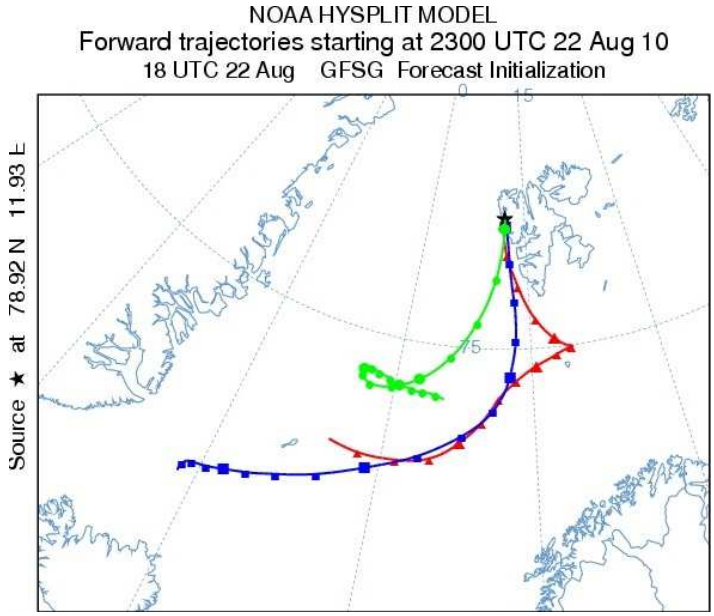

Figure 5.2: *Forecast trajectories for balloon no 2 from NOAA's Hysplit model. Red, blue and green represent 500 m, 1500 m and 3000 m, respectively. The small markers represent 6-hour intervals (placed at 06, 12 and 18 UTC), while the larger ones represent 24-hour intervals stating at midnight (UTC).*

This makes sense, because the height of the blue trajectory is closer to the floating altitude of the balloon.

The first 65 hours (2 days and 17 hours) in figure 5.2 can be compared with balloon no 2 in figure 4.4. The balloon trajectory is most similar to the green trajectory, and it has also almost the same curve, which starts after approximately 12 hours in both trajectories. As seen by the colors of the balloon trajectories (and in figure 4.3), the balloon had three soundings between 850 m and 6000 m, approximately, and therefore changed altitude from the floating altitude at 2000 m. This might be the reason why the balloon trajectory is more similar to the green than the blue trajectory, even when the blue trajectory is closer in altitude.

Figure 5.3's first 76 hours (3 days and 4 hours) can be compare with the third balloon in figure 4.4. All the forecast trajectories are quite similar to the shape of the balloon trajectory the first 44 (green)-56 (blue and red) hours, but the actual balloon has had a higher velocity, and is at almost the same place after only 30 hours. After this the red trajectory separates from the blue and green trajectories, and after another 24 hours the blue and green trajectories separate. The balloon is closest to the green trajectory. The last hours the balloon turns more north than the green trajectory, and they are not that similar anymore.

The first 60 hours (2 days and 12 hours) from figure 5.4 can be used to compare with balloon no 4 in figure 4.4. The green and blue forecast trajectories

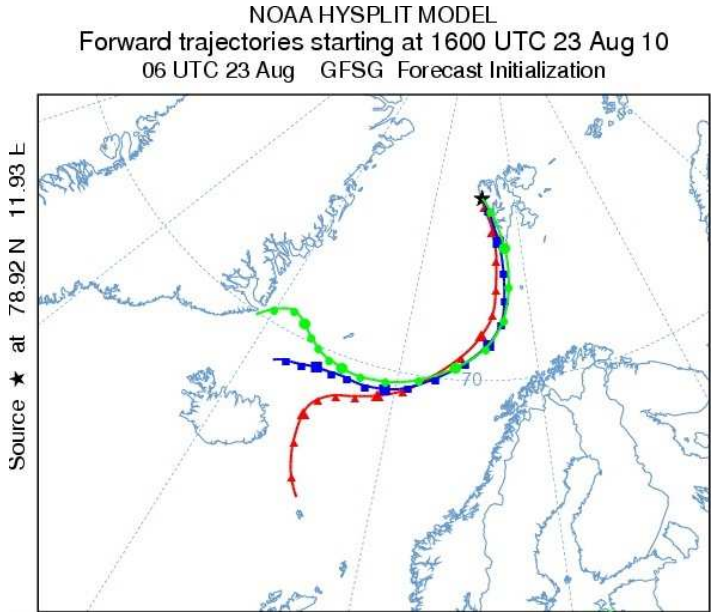

Figure 5.3: *Forecast trajectories for balloon no 3 from NOAA's Hysplit model. Red, blue and green represent 500 m, 1500 m and 3000 m, respectively. The small markers represent 6-hour intervals (placed at 06, 12 and 18 UTC), while the larger ones represent 24-hour intervals stating at midnight (UTC).*

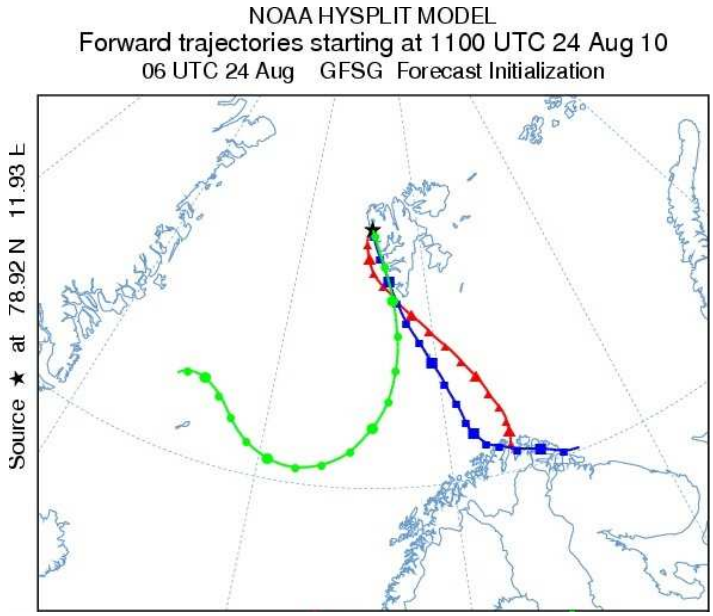

Figure 5.4: *Forecast trajectories for balloon no 4 from NOAA's Hysplit model. Red, blue and green represent 500 m, 1500 m and 2000 m, respectively. The small markers represent 6-hour intervals (placed at 06, 12 and 18 UTC), while the larger ones represent 24-hour intervals stating at midnight (UTC).*

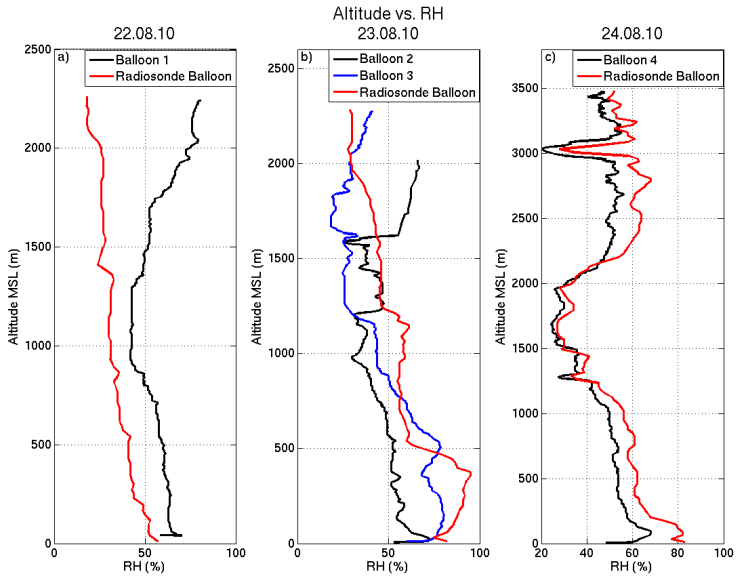

Figure 5.5: *Altitude vs. RH for balloon no 1-4. a) shows balloon 1 released 00:02 (22:02 UTC 21.08.2010) with the radiosonde balloon released 22.08.2010. b) shows balloon 2 released 00:55 (22:55 UTC 22.08.2010), and balloon 3 released 18:27 (16:27 UTC 23.08.2010), with the radiosonde balloon released 23.08.2010. c) shows balloon 4 released 12:47 (10:47 UTC 24.08.2010) with the radiosonde balloon released 24.08.2010.*

are almost exactly the same as the balloon trajectory the first 12 hours (approximately), but the blue trajectory is closest in time. For the rest of the duration time, the balloon trajectory is most similar to the green forecast trajectory, which would be expected since it is also closest in altitude.

5.2 CMET balloon ascent vs. radiosonde balloon

Figure 5.5-5.8 shows the CMET balloons compared with the radiosonde balloon released the same day. Figure 5.5 shows the relative humidity, figure 5.6 shows the temperature, figure 5.7 shows the wind direction, and figure 5.8 shows the wind speed, all of them compared with height. The a) subplots shows balloon no 1 and the radiosonde balloon released approximately 12 hours later. The b) subplots shows balloon no 2 and 3 and the radiosonde balloon released approximately 11 hours before and 7 hours after, respectively. The c) subplots shows balloon no 4 and the radiosonde balloon released approximately on the same time. As seen from the c) subplots, the CMET balloon and the radiosonde balloon measured almost exactly the same values on temperature, relative humidity, wind speed and direction. The reason why the other CMET and radiosonde balloon values are so different, is probably because the CMET balloons and the radiosonde balloons were released

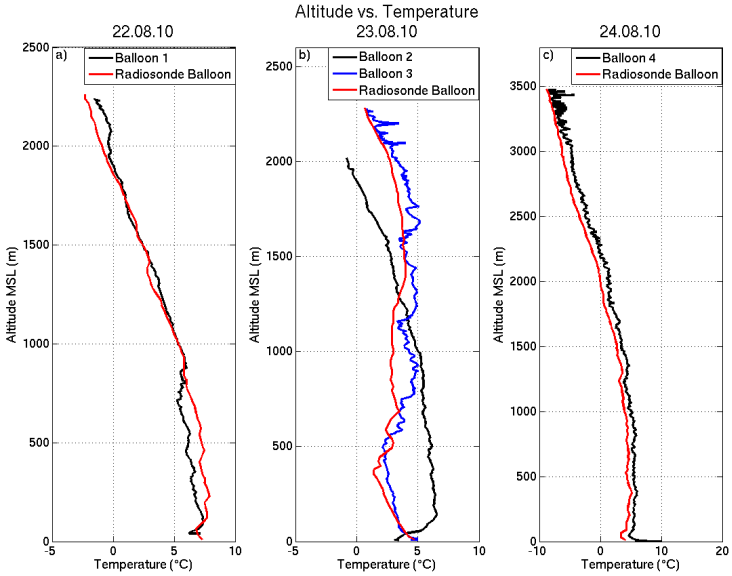

Figure 5.6: *Altitude vs. temperature for balloon no 1-4. a) shows balloon 1 released 00:02 (22:02 UTC 21.08.2010) with the radiosonde balloon released 22.08.2010. b) shows balloon 2 released 00:55 (22:55 UTC 22.08.2010), and balloon 3 released 18:27 (16:27 UTC 23.08.2010), with the radiosonde balloon released 23.08.2010. c) shows balloon 4 released 12:47 (10:47 UTC 24.08.2010) with the radiosonde balloon released 24.08.2010.*

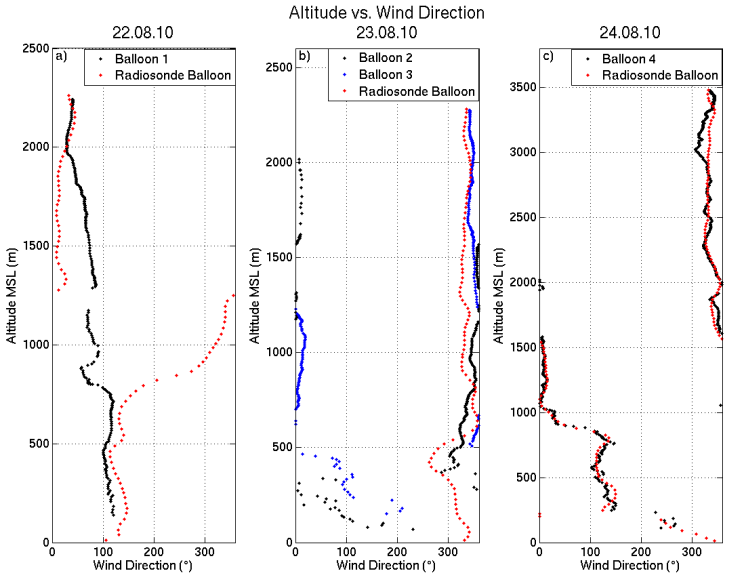

Figure 5.7: *Altitude vs. wind direction for balloon no 1-4. a) shows balloon 1 released 00:02 (22:02 UTC 21.08.2010) with the radiosonde balloon released 22.08.2010. b) shows balloon 2 released 00:55 (22:55 UTC 22.08.2010), and balloon 3 released 18:27 (16:27 UTC 23.08.2010), with the radiosonde balloon released 23.08.2010. c) shows balloon 4 released 12:47 (10:47 UTC 24.08.2010) with the radiosonde balloon released 24.08.2010.*

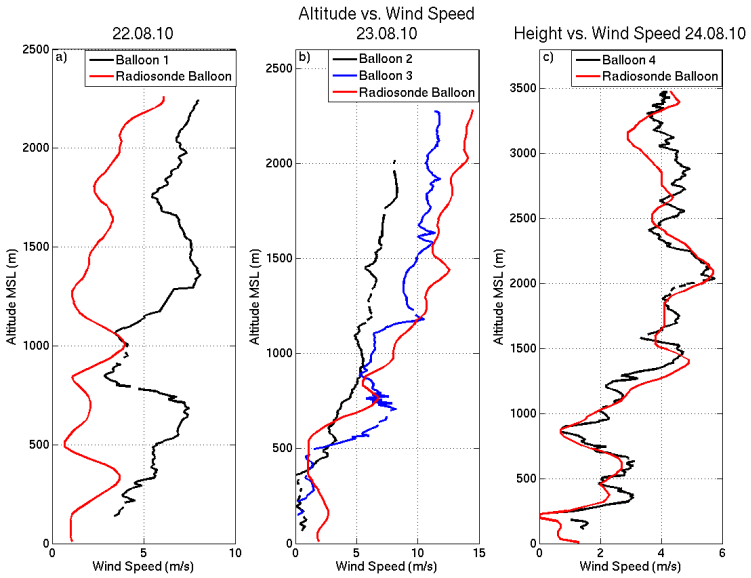

Figure 5.8: *Altitude vs. wind speed for balloon no 1-4. a) shows balloon 1 released 00:02 (22:02 UTC 21.08.2010) with the radiosonde balloon released 22.08.2010. b) shows balloon 2 released 00:55 (22:55 UTC 22.08.2010), and balloon 3 released 18:27 (16:27 UTC 23.08.2010), with the radiosonde balloon released 23.08.2010. c) shows balloon 4 released 12:47 (10:47 UTC 24.08.2010) with the radiosonde balloon released 24.08.2010.*

several hours apart. It seems like the sensors on the CMET balloons are well calibrated.

5.3 Curtain plots

Figure 5.9-5.12 shows curtain plots for balloon 1-4. These curtain plots are the result of interpolation of a) specific humidity, b) potential temperature, c) wind direction, and d) wind speed, with respect to flight duration and altitude. Because of the interpolation, the curtain plots are not perfect, especially places with few data points. Also plotted in each of the subplots is the balloon trajectory with respect to flight duration and altitude.

5.3.1 Balloon no 1

The specific humidity in figure 5.9 a) decrease with altitude, except for approximately the first 7 hours where the humidity is constant (and even increasing in some areas). The potential temperature in subplot b) has a similar structure with increasing potential temperature with altitude, except for the first 5 hours where the potential temperature is almost constant. This means that the air at the first 5-7 hours has been exposed to mixing from lower altitudes.

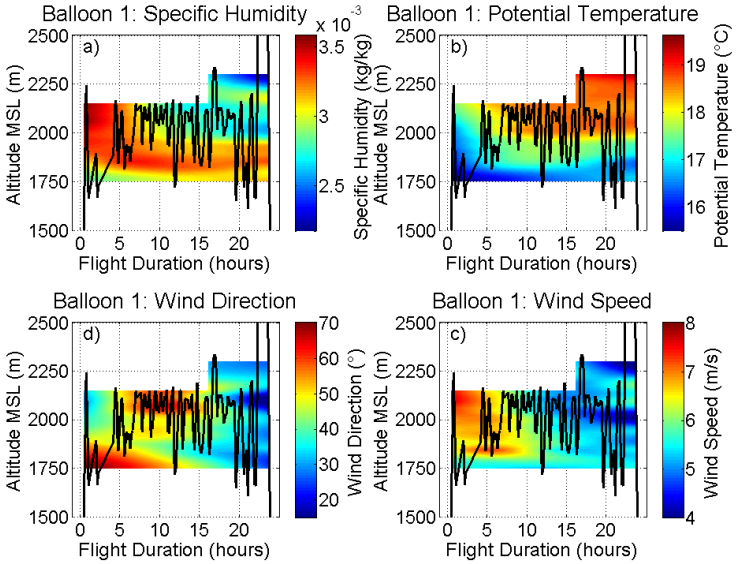

Figure 5.9: *Balloon no 1: a) specific humidity, b) potential temperature, c) wind direction, and d) wind speed interpolated with respect to flight duration and altitude. The black line is the balloon trajectory with respect to flight duration and altitude.*

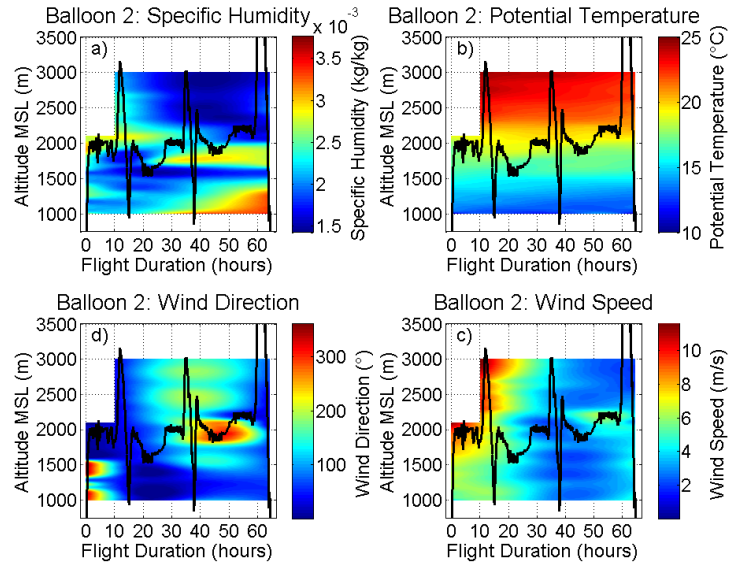

Figure 5.10: *Balloon no 2: a) specific humidity, b) potential temperature, c) wind direction, and d) wind speed interpolated with respect to flight duration and altitude. The black line is the balloon trajectory with respect to flight duration and altitude.*

The wind direction in subplot c) starts from north north-east and then turns more towards east north-east. The wind direction varies with altitude the first 5 hours, but after that it is more or less constant with altitude (the scale goes only between 15 and 70 degrees).

In subplot d) it is possible to see the wind speed decreases with flight duration, except for the 50 lowest m (between 1750 m and 1800 m), where the wind speed stays relatively constant (it is lower than aloft the approximately first 10 hours).

5.3.2 Balloon no 2

The specific humidity in figure 5.10 a) is quite low except for two cells around 1700 m to 2000 m (and also a small area between 1000 m and 1400 m at the end of the flight duration, which might not be really reliable, because of few data points). Parts of the cells have also slightly lower potential temperature then the rest of the air at the same altitude, as shown in subplot b). Still the potential temperature increases relatively constant with altitude throughout the flight. There might be some low level mixing where the cells are.

The reason for the loop in the trajectory shown in figure 4.4 is not hard to see looking at subplot c). The wind direction is relatively constant, except between 30 and 60 hours where the wind turns (there are also some areas at the beginning of the balloons ascent). The contrast is strongest at 2000 m, but there are also cells with turning air below and above. The balloon has probably passed air with anti-cyclonic properties.

The wind speed in subplot d) is mainly constant with altitude except for the first 20 hours where the wind speed increases with height. After 25 hours the wind speed is relatively constant during the flight. There is an area just after the loop (following the balloon trajectory) where the wind speed is higher than the wind speed at other altitudes at the same time.

5.3.3 Balloon no 3

The specific humidity in figure 5.11 a) is low and constant with altitude in the beginning of the flight. After 30 hours the specific humidity starts to change towards higher values, first mainly in lower altitudes, but in the end of the flight the high specific humidity has also reached the air aloft as well. The potential temperature seen in subplot b), shows similar structure as the specific humidity, but with opposite values. The potential temperature is high in the beginning, but decreases during the flight. There is a great possibility that the vertical mixing from lower altitudes at the last part of the flight is

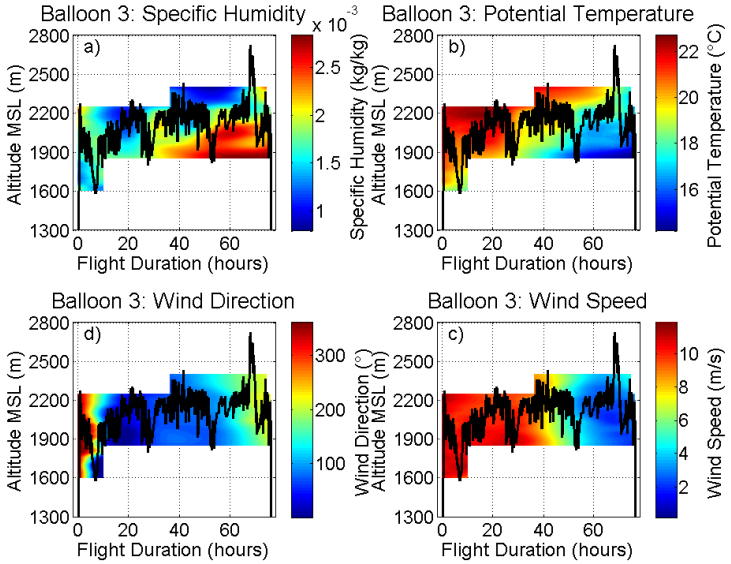

Figure 5.11: *Balloon no 3: a) specific humidity, b) potential temperature, c) wind direction, and d) wind speed interpolated with respect to flight duration and altitude. The black line is the balloon trajectory with respect to flight duration and altitude.*

caused by turbulence close to the high mountains at Greenland's coast.

The wind direction in subplot c) is also quite constant with altitude. The wind direction changes from north via north-east to east, then south to south-west, as also shown in figure 4.4.

Subplot d) shows that the wind speed for the approximately first 40 hours is constant with both altitude and flight duration. After this, the wind speed is still constant with altitude, but it changes fast to lower values, which it continued with for the rest of the flight.

5.3.4 Balloon no 4

Figure 5.12 a), consists mainly of cells with different specific humidity. There are three cells with low specific humidity, located between 1800 m and 2200 m (at the beginning of the flight), at 2500 m (at 20-30 hours) and between 2500 m and 2900 m (at the end of the flight). There are also three cells of relatively high specific humidity located between 2200m and 3000m (at the beginning of the flight), at 2500 m (at 30-50 hours) and between 2000 m and 2400 m (at the end of the flight).

The potential temperatures in subplot b) also show signs of these cells, with mostly lower potential temperature where the humid cells are located, and vice versa (except for the approximately first 7 hours).

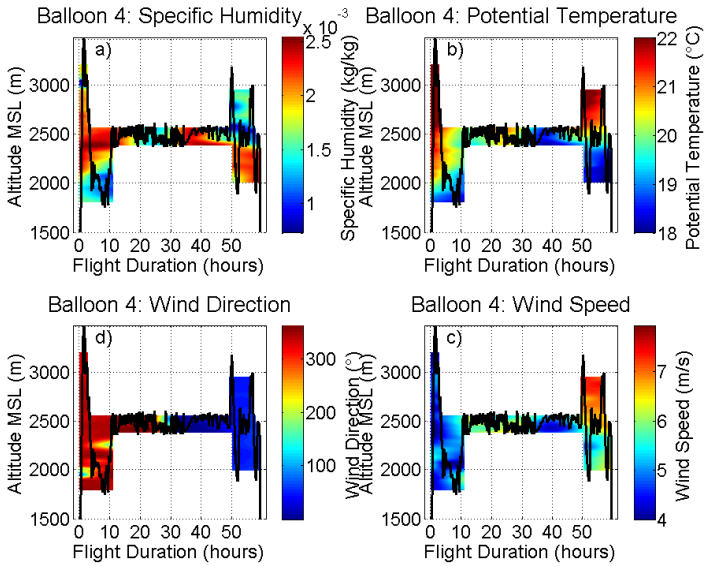

Figure 5.12: *Balloon no 4: a) specific humidity, b) potential temperature, c) wind direction, and d) wind speed interpolated with respect to flight duration and altitude. The black line is the balloon trajectory with respect to flight duration and altitude.*

The wind direction in subplot c) is almost constant with altitude, and the wind direction changes from north-west to north-east, during the flight. The wind speed in subplot d) is relatively low and constant for the whole flight, except for the areas where the two last low humid cells are located, where the wind speed is noticeable higher.

It is hard to say anything about mixing for the air around this balloon, because the area that is interpolated is so small. It seems to be some mixing from lower altitudes where the relatively humid cells are, and there might even be some mixing from aloft where the dry cells are.

5.4 CMET balloons vs. FLEXPART

Figure 5.13-5.20 shows the model run and the CMET balloon for each of the 4 balloons. The model was run with 50 imaginary air parcels released from each altitude. All of them released from a 10 km * 10 km box surrounding the longitude and latitude point the balloon had at the top of its ascent, and at the same time. The red trajectories are the results of the model run from the same altitude as the balloon had at the top of its ascent, while the other colors represent model runs from lower and higher altitudes. These figures are made to see if the FLEXPART model spans the variability of the balloons values of relative humidity and potential temperature, when the model are run from all of the balloons altitudes. Figure 5.13, 5.15, 5.17 and 5.19 shows

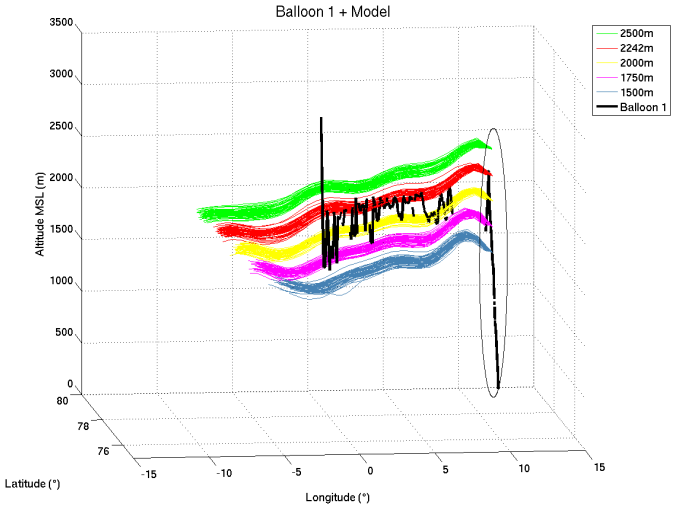

Figure 5.13: *Balloon and FLEXPART trajectories for balloon no 1, 21 (22:02 UTC) - 22 (22:50 UTC) August; showing longitude and latitude vs. altitude. The black circle points out the start of the balloon and model trajectories, the black line shows the balloon trajectory, the red lines shows the model run from the actual height the balloon had at its top, and the other colors shows the model runs from other altitudes.*

3-D plots which gives an overview of the longitude, latitude and altitude for each of the four balloons. The subplots in figure 5.14, 5.16, 5.18 and 5.20 shows, a) longitude vs. latitude, b) flight duration vs. altitude, c) flight duration vs. relative humidity and d) flight duration vs. potential temperature.

5.4.1 balloon no 1

Figure 5.14 a) shows that the balloon and model are really similar in the beginning and that they separate from each other at approximately (2 °E, 77.3 °N). Seen from the markers, this separation occurs just after 15 hours. Looking at subplot c), it is possible to see that the balloon and model have the same decreasing trend in relative humidity for the first 15 hours. For these hours, the model also spans the variation in relative humidity pretty vel. After 15 hours the trend of the balloon changes to increasing relative humidity, while the model keeps decreasing. This makes sense since this is the same time as the balloon and model separates in subplot a). The temperature from the model in subplot d) spans the balloon temperature very well, even after 15 hours.

5.4.2 balloon no 2

Subplot a) in figure 5.16 shows that the balloon and model are aligned, but that the balloon follows the yellow lines (2250 m) for the approximately first

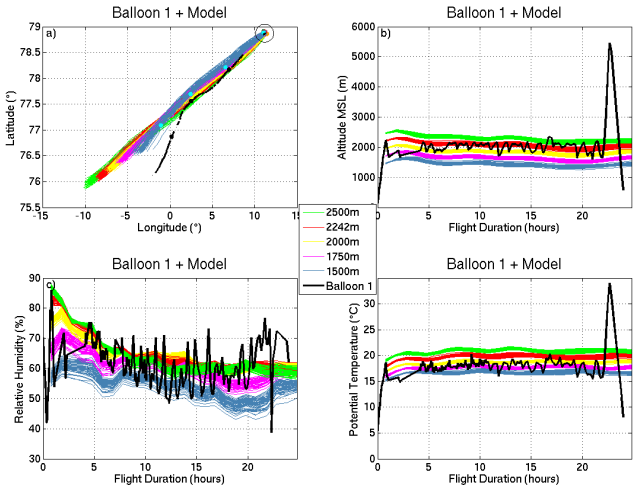

Figure 5.14: *Balloon and FLEXPART trajectories for balloon no 1, 21 (22:02 UTC) - 22 (22:50 UTC) August. a) longitude vs. latitude, b) flight duration vs. altitude, c) flight duration vs. relative humidity and d) flight duration vs. potential temperature. The black circle points out the start of the balloon and model trajectories, the black line shows the balloon trajectory, the red lines shows the model run from the actual height the balloon had at its top, and the other colors shows the model runs from other altitudes. The markers in subplot a) represent 6-hour intervals.*

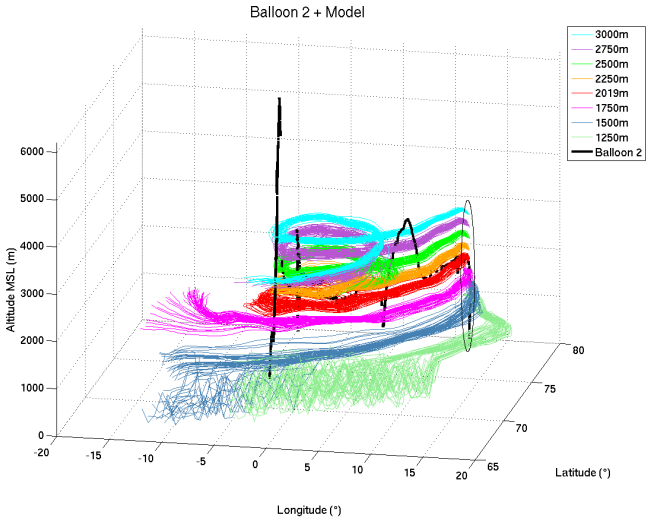

Figure 5.15: *Balloon and FLEXPART for balloon no 2, 22 (22:55 UTC) - 25 (15:24 UTC) August; showing longitude and latitude vs. altitude. The black circle points out the start of the balloon and model trajectories, the black line shows the balloon trajectory, the red lines shows the model run from the actual height the balloon had at its top, and the other colors shows the model runs from other altitudes.*

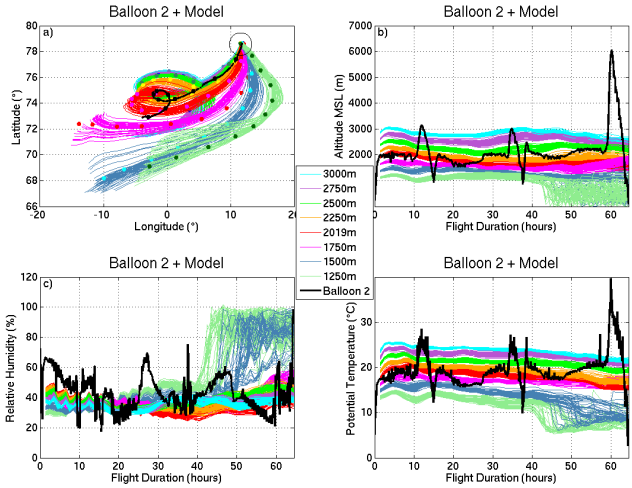

Figure 5.16: *Balloon and FLEXPART trajectories for balloon no 2, 22 (22:55 UTC) - 25 (15:24 UTC) August. a) longitude vs. latitude, b) flight duration vs. altitude, c) flight duration vs. relative humidity and d) flight duration vs. potential temperature. The black circle points out the start of the balloon and model trajectories, the black line shows the balloon trajectory, the red lines shows the model run from the actual height the balloon had at its top, and the other colors shows the model runs from other altitudes. The markers in subplot a) represent 6-hour intervals.*

24 hours, even though the altitude in subplot b) would imply the red lines (2019 m). The balloon has a loop just after 24 hours, which it uses approximately 26 hours on. The loop in the balloon values has a much tighter curl than the model, and this might be because of the sounding that was taken at approximately 35 hours. After the loop at 50 hours, the balloon and model are further apart, this might be because the air has moved. Looking at subplot b) just after 42 hours (second half of the loop in subplot a)) the lowest air masses from the model (1250 m and 1500 m) starts to sink and it seems that the air has reached the boundary layer, which has a lot of turbulent mixing. Subplot c) shows that at the same time, these air masses get relatively more humid. The balloon measurements reach also these high values of relative humidity when it falls down to the sea surface at the end. The temperatures in subplot d) also rise for the lowest air masses in the end, which is probably the effect of the sinking air in subplot b). It is possible to see that small changes in the balloon temperature have a great effect on the relative humidity. This might be the reason for that the modeled relative humidity does not span a big part of the balloons values; but because the altitude of the balloon is perfectly spanned, and almost just as good for the temperature, there is probably also another reason for this bad span.

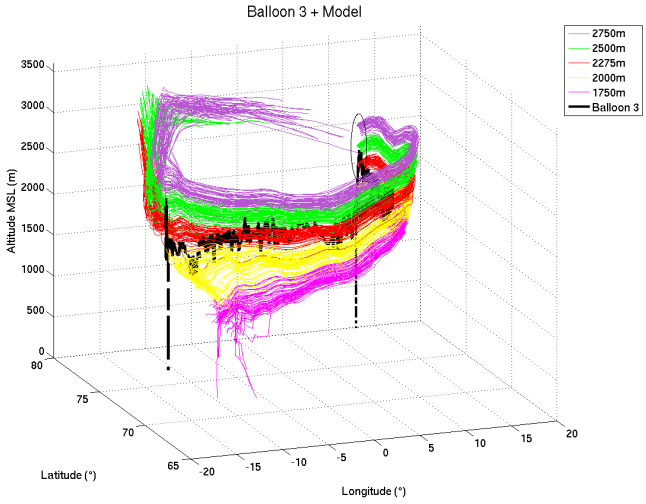

Figure 5.17: *Balloon and FLEXPART trajectories for balloon no 3, 23 (16:27 UTC) - 26 (20:15 UTC) August; showing longitude and latitude vs. altitude. The black circle points out the start of the balloon and model trajectories, the black line shows the balloon trajectory, the red lines shows the model run from the actual height the balloon had at its top, and the other colors shows the model runs from other altitudes.*

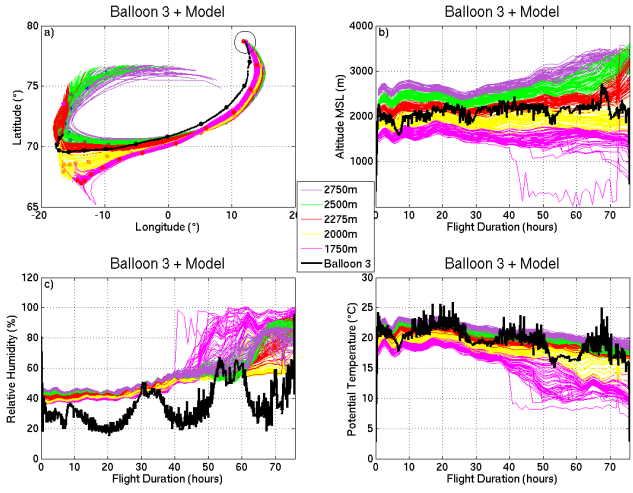

Figure 5.18: *Balloon and FLEXPART trajectories for balloon no 3, 23 (16:27 UTC) - 26 (20:15 UTC) August. a) longitude vs. latitude, b) flight duration vs. altitude, c) flight duration vs. relative humidity and d) flight duration vs. potential temperature. The black circle points out the start of the balloon and model trajectories, the black line shows the balloon trajectory, the red lines shows the model run from the actual height the balloon had at its top, and the other colors shows the model runs from other altitudes. The markers in subplot a) represent 6-hour intervals.*

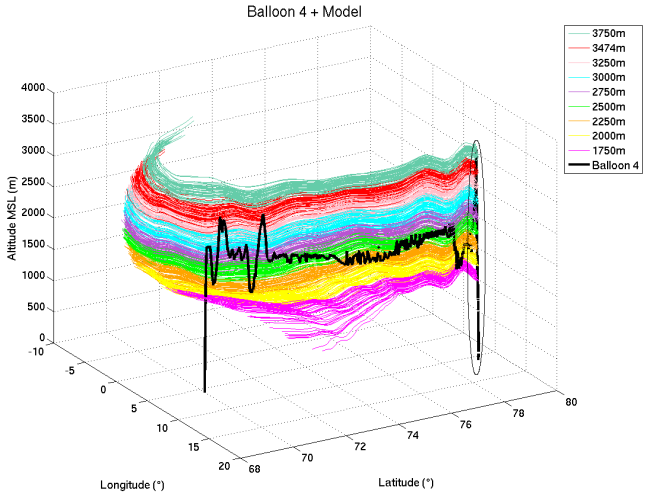

Figure 5.19: *Balloon and FLEXPART trajectories for balloon no 4, 24 (10:47 UTC) - 26 (22:18 UTC) August; showing longitude and latitude vs. altitude. The black circle points out the start of the balloon and model trajectories, the black line shows the balloon trajectory, the red lines shows the model run from the actual height the balloon had at its top, and the other colors shows the model runs from other altitudes.*

5.4.3 balloon no 3

Figure 5.18 a) shows that the balloon and model are quite close in the beginning and extremely close for the last 40 hours. As seen in subplot b) the modeled altitude for the highest air masses are rising (2750 m, 2500 m and 2275 m), and that the lowest air mass is sinking (1750 m) at the end of the run. As a consequence of this, most of the air masses also have a sinking temperature towards the end, as seen in subplot d). In subplot c) it seems like the lowest air masses from the model reaches the boundary layer in the end (after approximately 45 hours), just like balloon no 2. For balloon no 3 it is even more clear that small changes in the temperature makes big changes in the relative humidity. Here it is possible to see that there are some diurnal variation in the relative humidity (higher values during the night) and potential temperature (lower values during the night). The modeled humidity spans little of the balloon values. One reason for that the span is worse than for balloon no 2, is that the potential temperature span is not as good for no 3.

5.4.4 balloon no 4

Subplot a) in figure 5.20 shows that the balloon trajectory separates from the model at approximately (15 °E, 77 °N), which is equal to 10 hours seen from the markers. As seen from subplot b) this is just after the first sounding. The balloon rejoins with the model again at approximately (16 °E, 75.5 °N), but then it follows the model run from 1750 m. The reason for this might

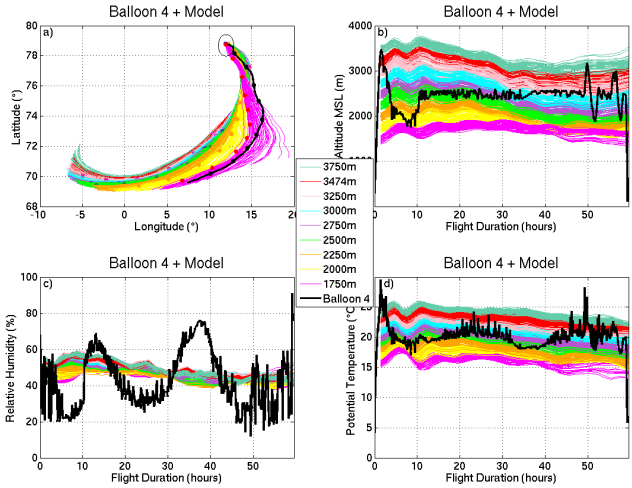

Figure 5.20: *Balloon and FLEXPART trajectories for balloon no 4, 24 (10:47 UTC) - 26 (22:18 UTC) August. a) longitude vs. latitude, b) flight duration vs. altitude, c) flight duration vs. relative humidity and d) flight duration vs. potential temperature. The black circle points out the start of the balloon and model trajectories, the black line shows the balloon trajectory, the red lines shows the model run from the actual height the balloon had at its top, and the other colors shows the model runs from other altitudes. The markers in subplot a) represent 6-hour intervals.*

be the sounding we took in the beginning, and when the balloon was finally stabilized at floating height the air masses had changed. In subplot b) the modeled air starts to sink after approximately 20 hours, but the balloon is held at a constant float altitude; still the model spans all of the balloons values. This is definitely not the case in subplot c); here the relative humidity variation of the balloon is much greater than the variation of the model. As for balloon no 3 the data seems to show diurnal variation in the relative humidity, with higher values during the night. As seen in subplot d) there are also some diurnal variation in the potential temperature (lower values at night), even though they are quite small. The span of the modeled relative humidity is not good, but it is at least better than for balloon no 3.

5.5 Relative Horizontal Transport Deviation

Before calculating the relative horizontal transport deviation, figure 5.21 was made. Each of the subplots contains the model run for 50 imaginary air parcels for the balloon's float altitude, the balloon flight, and a line with constant altitude, the same altitude as the balloon's float altitude. One subplot for each balloon, and they are plotted as flight duration vs. altitude. The blue and pink lines are two random chosen model trajectories that are used as the model run in figure 5.22.

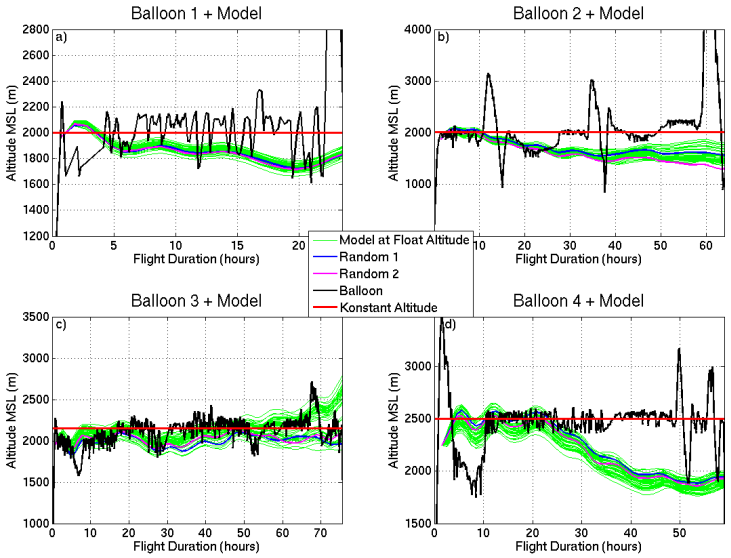

Figure 5.21: *Balloon and model together in each subplot, plotted as flight duration vs. altitude. a) balloon 1, b) balloon 2, c) balloon 3, and d) balloon 4. The green lines represent the model run with 50 imaginary air parcels, the blue and pink line are two of these trajectories randomly chosen. The black line is the balloon, and the red line is a line with constant altitude.*

The left column in figure 5.22 shows the balloon and two random model trajectories, calculated from the main balloon floating altitude, plotted as longitude vs. latitude for all four balloons. The right column in figure 5.22 shows the relative trajectory error, also known as RHTD, calculated for each balloon as a percentage of the balloon trajectory length, and plotted for each hour. The markers in all the subplots represent 3-hours intervals. The trajectories are not the complete trajectories for the balloons, and therefore the RHTD calculated are only for the first part of the trajectories. The reason for this is that the RHTD only measure the horizontal deviation, and can therefore only be calculated (with any meaning) when the air is not sinking or rising in comparison with the balloon. As shown in figure 5.21 the air stats to sink after some hours in all the subplots except c) (balloon 3). The trajectories in figure 5.22 for balloon no 3 are truncated to make it possible to compare it with the other balloons, while the rest of the balloons are truncated because of sinking air. The figure shows the 16 first hours for balloon no 1, 26 hours for balloon no 2, 30 hours for balloon no 3, and 24 hours for balloon no 4.

The RHTD for balloon no 1 is not really reliable, because the altitude of the balloon randomly oscillates between approximately 1700 m and 2200 m (at the time considered), and therefore only has the same height as the model

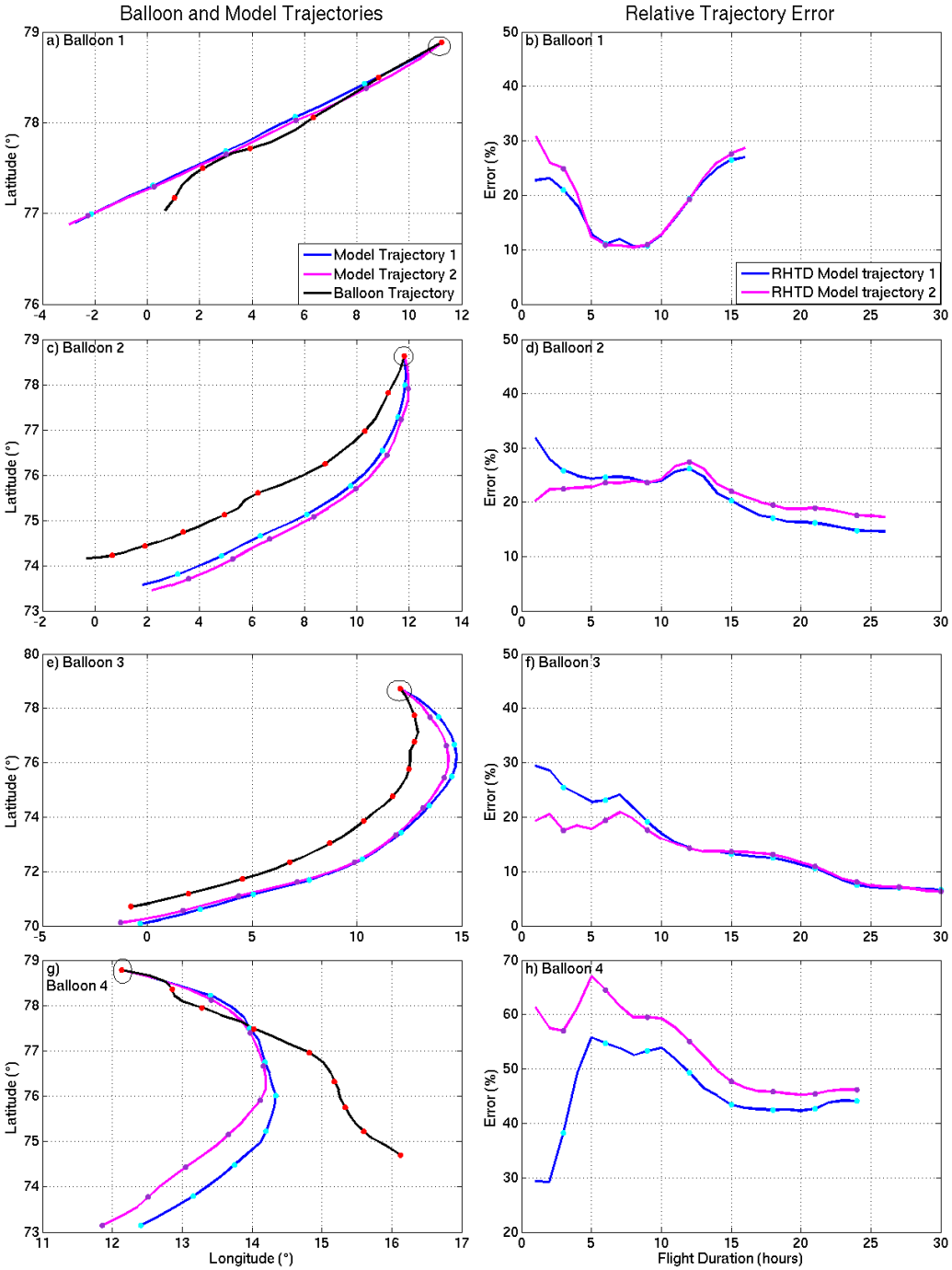

Figure 5.22: *The left column shows the truncated balloon and model trajectories plotted as longitude vs. latitude for all four balloons. The right column shows the Relative trajectory error/RHTD for the four balloons based on the truncated trajectories in the left column. The markers represent 3-hours intervals, and the black circle in the subplots in the left column represents the start of the trajectories.*

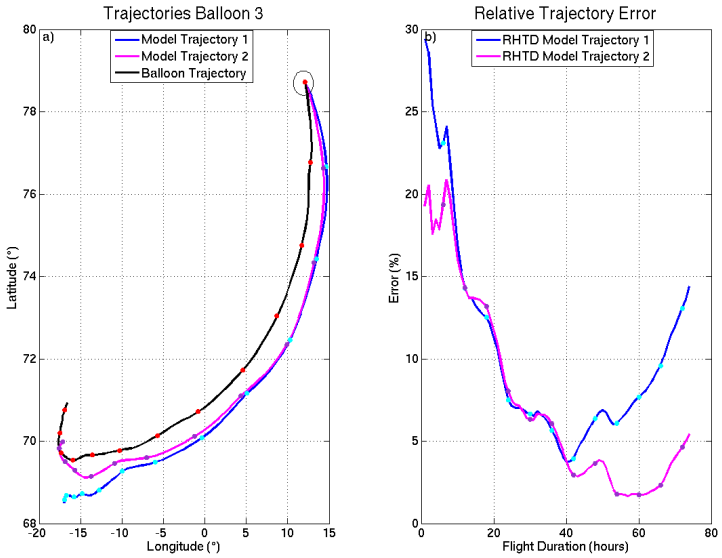

Figure 5.23: *a) full balloon and model trajectories plotted as longitude vs. latitude for balloon no 3. b) relative trajectory error/RHTD based on the trajectories in a), plotted as flight duration in hours vs. error in %. The markers represent 6-hours interval and the black circle in a) represents the start of the trajectories.*

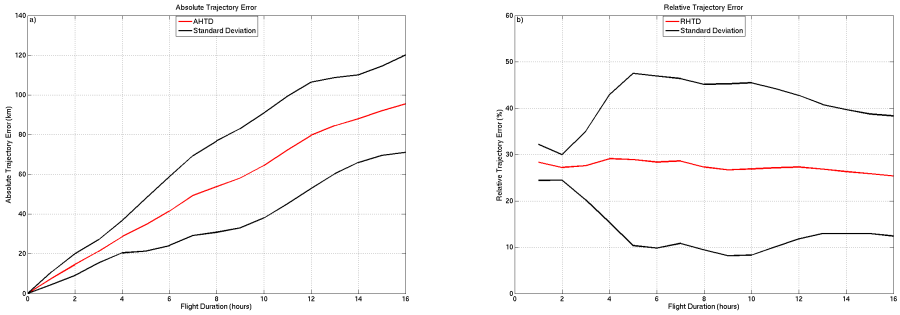

Figure 5.24: *The red lines show: a) average absolute horizontal deviation (AHTD) and b) average relative horizontal deviation (RHTD) for the first 16 hours of the four balloon flights (model trajectory 1 from figure 5.22 is used), both with respect to flight duration. The black lines show a single standard deviation above and below the mean errors.*

trajectories in its lower altitudes [1]. The RHTD for balloon no 2 is also calculated for some hours after the air starts to sink, because the balloon also descents in altitude for a while. The reason why the RHTD is so major in the beginning, is because the length of the balloon trajectory is so short at that time.

In figure 5.23 in subplot a) the total balloon and the two model trajectories

[1]Should have used the model run from 2100 m/ 2150 m, but when this was discovered FLEXPART was down and it has been since.

for balloon no 3 is plotted as longitude vs. latitude, and in b) the calculated RHTD for the whole flight is plotted for each hour. The markers in both subplots represent 6-hours intervals. The model and the balloon are very close, and thus the calculated RHTD is really small.

Figure 5.24 shows the average AHTD and RHTD for the first 16 hours for the four balloons and model trajectory 1 from figure 5.22, with respect to flight duration. A single standard deviation above and below the mean errors are also shown. The increase in AHTD with time is approximately linear, while the RHTD is relative constant. It should be said that the calculated results would have been more reliable with several more trajectories.

5.6 Interpolated CMET balloon data vs. FLEXPART

The modeled trajectories from FLEXPART are programmed to follow constant theta surfaces; hence it would be best to interpolate the data with respect to potential temperature and flight duration. As seen from figure 5.25 the model does not follow constant potential temperature (except for balloon 1), so then the interpolation was done with respect to altitude and flight duration instead.

Shown in figure 5.26-5.29 are the interpolated CMET balloon data, based on the interpolation technique shown in section 5.3, and the FLEXPART model run. In these figures the model was run with only 5 imaginary air parcels in total, released from 2-3 altitudes. The subplots in the figures shows a) longitude vs. latitude, b) flight duration vs. altitude, c) flight duration vs. relative humidity, and d) flight duration vs. potential temperature. The interpolated balloon data are only taken from the area within the interpolation in figure 5.9-5.12, because there are too few data points outside this area, and thus the interpolated trajectory would not be valid in these cases. Subplots a) should really be calculated by integrating the wind vectors, but because the interpolated balloon trajectories are taken from constant altitudes the wind shear can be ignored. Thus the trajectories can be seen as valid. Subplots b) are made to demonstrate the difference in altitude for the interpolated trajectories and the model, even though they are released from the same height. It shows also which model run, and at which time interval, this model run can be compared with the interpolated balloon trajectories.

5.6.1 Balloon no 1

Figure 5.26 a) shows that the interpolated balloon data and model runs, for all altitudes, are almost identical the first 6 hours. After this the model- and balloon trajectories separate from each other.

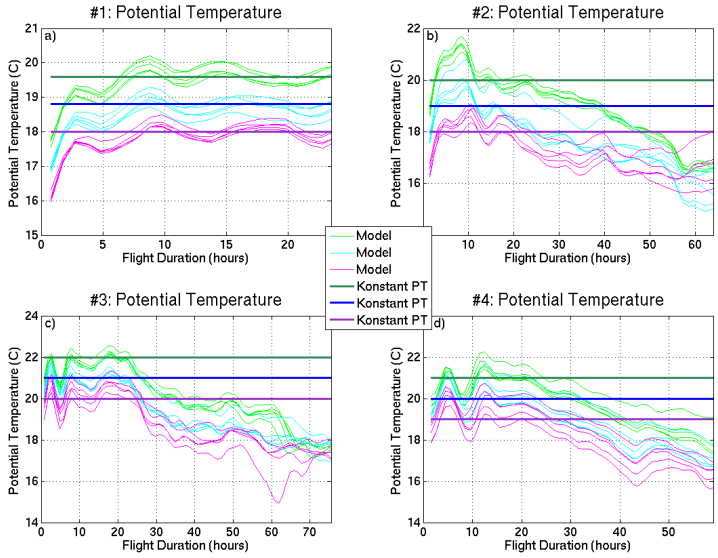

Figure 5.25: *Flight duration vs. potential temperature. The thin trajectories are from FLEXPART and the thicker lines are constant potential temperatures. a) balloon no 1, b) balloon no 2, c) balloon no 3 and d) balloon no 4.*

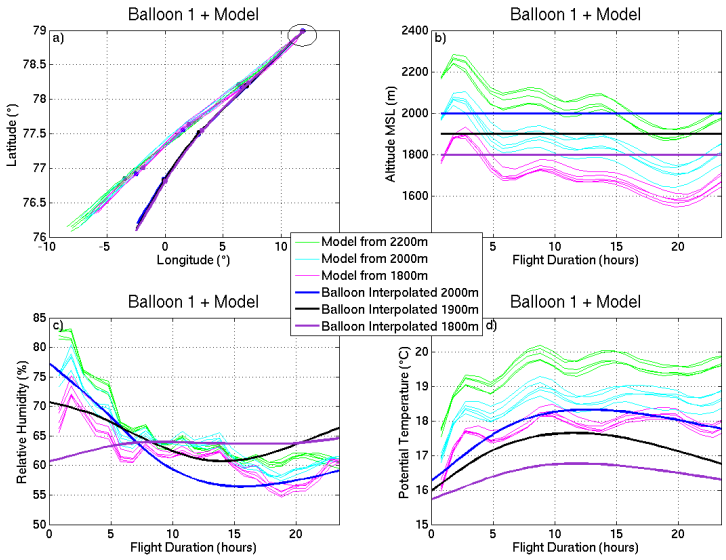

Figure 5.26: *Interpolated trajectories from balloon no 1 and the model run. a) longitude vs. latitude, b) flight duration vs. altitude, c) flight duration vs. relative humidity, and d) flight duration vs. potential temperature. The black circle points out the start of the balloon and model trajectories, and the markers represent 6-hour intervals.*

Subplot b) shows that the interpolated balloon at 2000 m and 1800 m almost follow the modeled trajectories from the same altitude approximately for the first 5 hours. Then the modeled air parcels sink, and the interpolated balloon data starts to follow the modeled air from 2200 m and 2000 m, respectively. This might be the reason for the separation in a).

The blue trajectory in subplot c) follow the modeled air from the same altitude really well the first 7 hours, after this the interpolated trajectory and the model (it should be following the light green trajectories) have opposite trends until 18 hours into the flight where the trends become similar again. The black trajectory shall according to b) follow the pink model run the first 3 hours, then follow the light blue model lines between 4 and 14 hours, and then the light green model lines between 17 and 21 hours. It starts really well the first 10 hours, when it pretty much exactly follows the model. After 10 hours it is still good, and follows at least the trend of the model. The purple trajectory is not good the first 5 hours, but between 5 and 14 hours it follows the model exactly. The last hours also the purple trajectory follows the model trend.

Subplot d) shows that the potential temperature calculated by FLEXPART generally is too high compared to the interpolated balloon data.

5.6.2 Balloon no 2

Figure 5.27 a) shows that the model and the interpolated balloon data from 1800 m and 2000 m follow a similar trend, but that the trajectories do not overlap exactly. The rest of the interpolated balloon trajectories turn the opposite way of the model where the loop is located, and therefore do not follow any of the model runs. The reason why the trajectories from the model and the interpolated balloon data do not match exactly might be the sinking air shown in subplot b), and the fact that none of the balloon trajectories follow the model's altitude exact (same reason as in figure 5.26).

The blue and green trajectory in subplot c) should follow the model runs for the first 10 and 15 hours, respectively, which is does not do at all (the blue trajectory might follow the modeled trend the first 10 hours). The purple line should follow the model, but at different altitudes, throughout the flight. It is close to the model between 5 and 22 hours, the trend is opposite of the model from 22 to 48 hours, and then the trend changes and becomes similar to the model runs the last hours. The yellow and red trajectory should follow the model runs from approximately 15 hours and 28 hours, respectively. Both the yellow and red line is actually most similar to the model the first 30 hours, even though the trajectories are not in the same altitude as the model. The yellow line is similar to the model the first 30 hours, after this the trajectory's trend in the relative humidity is opposite of the modeled trend, but at 56 hours the interpolated balloon and model

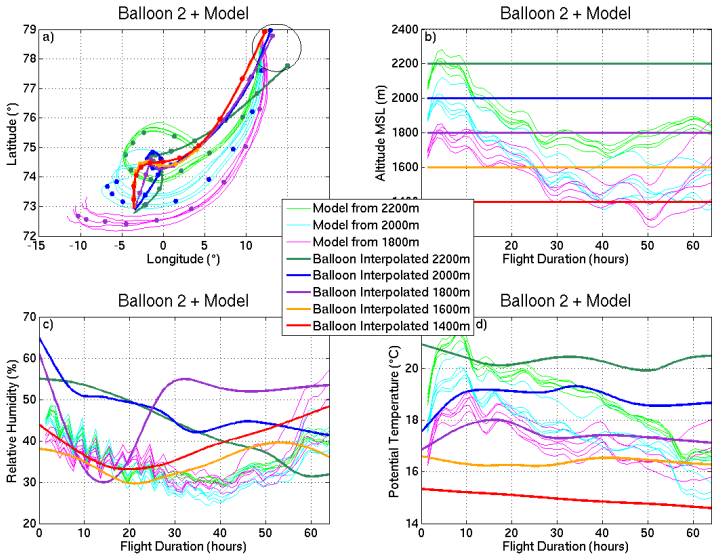

Figure 5.27: *Interpolated trajectories from balloon no 2 and the model run. a) longitude vs. latitude, b) flight duration vs. altitude, c) flight duration vs. relative humidity, and d) flight duration vs. potential temperature. The black circle points out the start of the balloon and model trajectories, and the markers represent 6-hour intervals.*

are similar again. The red line almost follows the trend of the same modeled altitude after 30 hours, and has very similar values as the model after 55 hours.

The potential temperature in subplot d) shows a closer resemblance between the interpolated balloons and the model runs than the relative humidity in c). The potential temperature to the interpolated data is also here (as in figure 5.26) a little lower than the modeled data. That is why the balloon trajectories seem to follow the model best just after they have separated in altitude, because the modeled potential temperature also decreases.

5.6.3 Balloon no 3

The interpolated data from balloon no 3, gives the balloon trajectories that are most similar to the model, as seen in figure 5.28 a). The resemblance is actually closer after the first the first 24 hours, and after another 12 hours they match almost perfectly.

As seen in subplot b) the modeled air does not sink, so that the balloon trajectories and the model stay in the same altitude for the whole flight duration, which makes it easier to compare the balloon and the model in the other subplots.

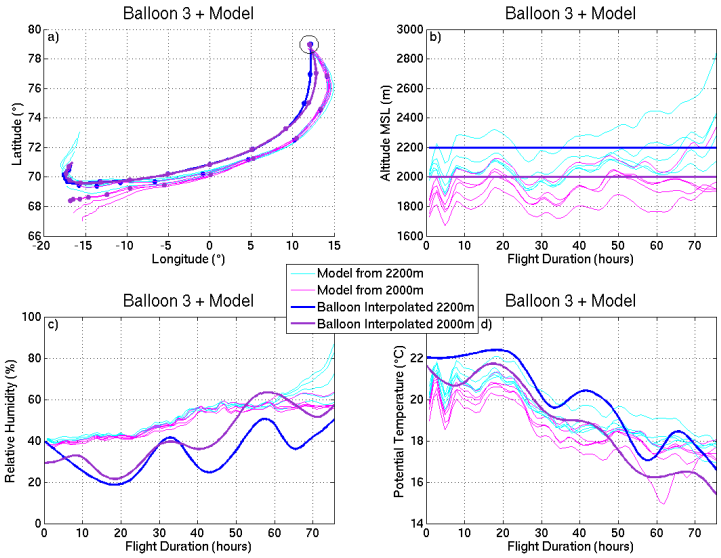

Figure 5.28: *Interpolated trajectories from balloon no 3 and the model run. a) longitude vs. latitude, b) flight duration vs. altitude, c) flight duration vs. relative humidity, and d) flight duration vs. potential temperature. The black circle points out the start of the balloon and model trajectories, and the markers represent 6-hour intervals.*

The relative humidity from the balloon data in subplot c) is generally to low in comparison with the model, but at least the average trend of the balloons follow the trend of the model. The potential temperature in subplot d) is quite similar for the interpolated balloons and the model throughout the flight.

5.6.4 Balloon no 4

Only one trajectory is shown in figure 5.29, because balloon no 4 has such a narrow band that can be interpolated (as seen in figure 5.3). Subplot a) shows that the trajectories from the interpolated balloon data and model have close resemblance the first 12 hours, before they separate. The model's velocity is generally higher than the balloon's velocity, so when the direction of the balloon changed after approximately 18 hours later (30 hours into the flight), the balloon turns towards a place the model had been several hours before.

Subplot b) shows that the balloon and model stays in the same altitude the first 28 hours, before the modeled air parcels start to sink.

The relative humidity of the balloon oscillates over the modeled data, and the oscillations become bigger during the flight, as seen in subplot c). The oscillations are also shown in the potential temperature in subplot d), even though

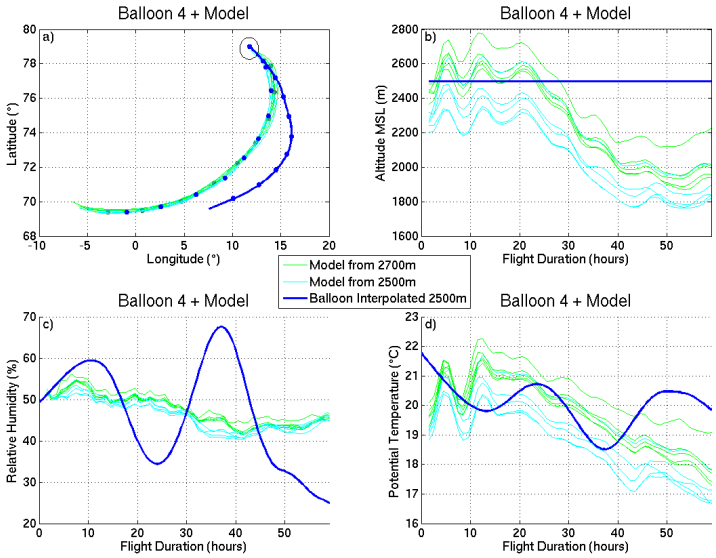

Figure 5.29: *Interpolated trajectories from balloon no 4 and the model run. a) longitude vs. latitude, b) flight duration vs. altitude, c) flight duration vs. relative humidity, and d) flight duration vs. potential temperature. The black circle points out the start of the balloon and model trajectories, and the markers represent 6-hour intervals.*

the oscillations are much smaller, and the potential temperature spanned by the model are much greater, than the span of the relative humidity in c). The interpolated data follow the model even after 30 hours, and it is hard to see that the balloon and model separate in altitude (except for maybe after 45 hours).

Chapter 6

Discussion and Conclusions

6.1 How is the relationship between the different plots for each balloon?

6.1.1 Balloon no 1

Figure 5.26 shows that the velocities of the balloon and model are quite similar, while figure 5.22 shows that the velocity is very similar in the start, but when the balloon's velocity decrease after approximately 9 hours (which is also shown in figure 5.9), the model keeps the same higher wind speed. Figure 5.14 shows that FLEXPART's wind speed at lower altitudes is more similar to the balloon's velocity than the wind speed at higher altitudes, where the balloon actually is.

The balloon and model separates after some time, but not at the same hour when looking at the real and the interpolated balloon (as seen in figure 5.14 and 5.26). The interpolated balloon separates from the model approximately 9 hours before the real trajectory (6 hours before when looking at the floating altitude in figure 5.22). The modeled relative humidity values are really good in comparison with the balloon in both figures (5.14 and 5.26) before the split. After the separation the resemblance is not that close, but the similarity is greater in some altitudes than others, as shown by the purple trajectory in figure 5.26. This means that the relative humidity probably varies in the horizontal direction.

The potential temperature from the model are generally higher than the potential temperature measured by the balloon (as shown in figure 5.14 and 5.26), and it does not seem too affected by the separation of the trajectories. This might mean that the potential temperature do not vary in the horizontal direction.

6.1.2 Balloon no 2

The horizontal wind speed modeled for balloon no 2 is approximately the same as the balloon measured for the first 24 hours (just a bit slower the

first 12 hours as shown in figure 5.22) In the balloon's trajectory loop, the measured velocity is less than the modeled.

The spanned relative humidity from FLEXPART is a bit too narrow for the real balloon in figure 5.16, and also compared with the interpolated balloon in figure 5.28 (where there is hard to see any resemblance at all). The biggest maxima in the relative humidity are at the same time as the relative humid cells in figure 5.10. These cells might be hard for the model to predict, which makes the calculated relative humidity too narrow.

The modeled potential temperature seems to be almost perfect compared with the real balloon, but with respect to the interpolated balloon the model seems to exaggerate the potential temperature a few degrees. The reason for this might be because the interpolated trajectories pass through the cells with slightly lower potential temperature, while the real balloon does not stay in the cells for a long period of time. As for the cells with higher relative humidity, the cells with lower potential temperature might be hard to predict.

6.1.3 Balloon no 3

Shown in figure 5.18 and 5.28 there is little vertical movements in the modeled air in the beginning, and the balloon's altitude does not change very much during the flight. That is probably the reason why the model has such a close resemblance to the balloon trajectories, both real and interpolated, especially after 30 and 36 hours, respectively. The reason why the similarity is better at the end is really hard to tell. Figure 5.28 shows very close resemblance between the modeled and the interpolated wind speed. On the other side, figure 5.23 shows that the modeled velocity for the approximately first 36 hours of the flight actually is too high compared with the balloon. After 36 hours the modeled wind speed also varies a lot between the different trajectories in the model, from too high to too low velocity.

Even though the air is relatively stable the first 40 hours of the flight (as seen in figure 5.11), the relative humidity does not seem to be well represented by the model (shown in figure 5.18 and 5.28). The average of the balloon's oscillations in both figures seems to have the same trend as the model, but the modeled values are generally too high. On the other hand, the balloon's potential temperature is quite well represented by FLEXPART in both figures (a bit narrow in figure 5.18).

6.1.4 Balloon no 4

Also for balloon no 4 the modeled wind velocity is over estimated, in comparison with the balloon and the interpolated balloon (figure 5.22, 5.20 and 5.29). The reason why the RHTD error is so large, is that the balloon follows

the modeled air at 1750 m instead of the air at its floating altitude at 2500 m. The interpolated balloon takes the same turn as the real balloon trajectory after 12 hours; away from the modeled trajectories (the real balloon starts to follow the 1750 m trajectories). The interpolated balloon values are almost exact as the real balloon data, because the balloon had a very stable floating altitude, at the exact height the interpolated balloon is interpolated from. The modeled air is sinking, so the balloon meats air from higher altitude during the flight.

As for balloon 3, the calculated relative humidity is not very similar to the balloon data (figure 5.20 and 5.29), but the average of the balloons oscillations seems to fit the model. The potential temperature from FLEXPART has a really close resemblance with the balloon values, even when the interpolated balloon data is in another altitude than the model. This might mean that there are small changes in potential temperature in the vertical direction.

6.2 Are the relationship the same for all the balloons, or does it change?

Generally the wind speed for almost all the balloons seems to be over exaggerated (except for balloon no 3 where it is really good). How good the model calculates the trajectories varies a lot between the balloons. The RHTD calculated for the first hours of each balloon flight varies between approximately 7 % (balloon no 3) and 47 % (balloon no 4) at the end of the calculations (see figure 5.22). The average AHTD and RHTD (from figure 5.24) is calculated the same way as in the paper by Riddle et al. (2006). The average errors calculated by Riddle are within two percentage points of 25 % (with 0.36° resolution in the ECMWF data), while the errors in this thesis is between 26.7 % and 29.1 % with an average of 27.7 % (with 0.2° resolution). Because the resolution used in this study is better than the resolution used by Riddle, the error here should have been smaller. The reason why it is not is most likely because the ensemble used in this study is too small. This is shown by removing the data from balloon no 4, which results in a drop in the average RHTD to 20.6 %. The error in this study might also be greater than the error found by Riddle, because the ECMWF model seems to be better at lower latitudes than close to the poles (Jung et al., 2005).

The relative humidity spanned by the model is generally too narrow (except for balloon no 1 before the split). One reason for this might be that the humidity sensor on the balloon is not perfectly calibrated, but figure 5.5 (especially subplot c) shows that the values of the CMET balloons and the radiosonde balloons are not that different. In other words, it would seem that the humidity sensors for the CMET balloons are well calibrated.

Another reason might be that the ECMWF data (which is used in the model) has too few measuring points in the balloon area (low resolution), so that the humidity and temperature in the ECMWF grid is a bit wrong. This means that FLEXPART calculates the relative humidity correct, but because the initial values are not totally precise the result also deviates slightly from reality. The potential temperature, from the model, resemblance the balloon much closer than the relative humidity, so it might just be the initial humidity that is a little incorrect.

6.3 Has the synoptic weather situation anything to do with the change in relationship?

It is hard to see if the synoptic weather situation had any impact on how good FLEXPART calculated the trajectories, because the weather situations were really similar during all of the four balloon flights.

The reason why FLEXPART calculates the trajectory for balloon no 3 best, is probably because the air stayed at a relatively constant height in the balloon's floating altitude, while the calculated air in the other cases had a tendency to sink.

6.4 Conclusions

The general conclusions from this project are:

The study shows that the wind speed used by FLEXPART is generally too high and that the relative humidity spanned by the model is generally too narrow. These errors might be originating from the ECMWF data. The potential temperature, on the other hand, is mostly really good.

How close resemblance the calculated trajectories from FLEXPART have with the balloons depends on the stability to the modeled air. More sinking air leads to bigger trajectory errors.

The calculated average RHTD for the first 16 hours is constant around 28 %, which are a few percentage points greater than in earlier studies (e.g. Riddle et al. (2006)). This would probably have been more reliable if the ensemble of the trajectories were greater.

Chapter 7

Further Work

When the curtain plots were made, we realized that we should have taken a lot more soundings to make the interpolated data more reliable. During the campaign in May this year five balloons were released, and two of them preformed automatically repeated soundings. This will improve the data for further analysis of the FLEXPART model.

During the campaign in May, the synoptic weather situation was also a bit different from the campaign in August last year, so it would be great to compare the FLEXPART run from the two campaigns and see if the synoptic weather situation has any impact on the calculation of the trajectories. It would also be possible to include the calculated RHTD from the new balloons in the average RHTD study and see how the results changes (if they do).

In further analyses it would be interesting to look at the Richardson number to study the vertical movements and mixing in the curtain plots.

In further studies it would be great to run FLEXPART with input from HIRLAM (High Resolution Limited Area Model) instead of ECMWF data, to see if HIRLAM predicts the wind better than ECMWF.

Bibliography

Bretherton, C. S. and R. Pincus (1995). Cloudiness and marine boundary layer dynamics in the astex lagrangian experiments. part i: Synoptic setting and vertical structure. *Journal of the atmospheric sciences 52*(16).

Businger, S. and R. Johnson (2000, January). Evolution in the design of a smart balloon for lagrangian air mass tracking. 11th Joint Conference on the Applications of Air Pollution Meteorology with the Air and Waste Management Association. `http://ams.confex.com/ams/annual2000/techprogram/paper_6279.htm`. Read 01.10.2010.

Businger, S., R. Johnson, J. Katzfey, S. Siems, and Q. Wang (1999). Smart tetroons for lagrangian air-mass tracking during ace 1. *Journal of Geophysical Research 104*(D9).

Christensen, J. (1997). The danish eulerian hemispheric model - a three dimensional air pollution model used for the arctic. *Atmospheric Environment 31*, 4169–4191.

Emanuel, K. A. and M. Živković-Rothman (1999). Development and evaluation of a convection scheme for use in climate models. *Journal of the atmospheric sciences 56*, 1766–1782.

Hojem, J. and I. Ohna (2010, Mars). Utslipp av klimagasser for norsk jordbruk og tiltak for å redusere dem. Technical report, Zero Emission Resource Organisation [ZERO]. `http://www.zero.no/publikasjoner/KLimagasser%20fra%20norsk%20jordbruk.p%df`.

Hole, L. R., J. H. Christensen, T. Ruoho-Airola, K. Tørseth, V. Ginzburg, and P. Glowacki (2009). Past and future trends in concentrations of sulphur and nitrogen compounds in the arctic. *Atmospheric Environment 43*, 928–939.

Holton, J. R. (2004). *An Introduction to Dynamic Meteorology* (4 ed.). Elsevier.

Jung, T., A. M. Tompkins, and M. J. Rodwell (2005). Some aspects of systematic error in the ECMWF model. *Atmospheric Science Letters 6*, 133–139.

Langmann, B., B. Duncan, C. Textor, J. Trentmann, and G. R. van der

Werf (2009). Vegetation fire emissions and their impact on air pollution and climate. *Atmospheric Environment 43*, 107–116.

Livik, G. (2011, February). An observational and numerical study of local winds in kongsfjorden, spitsbergen. Master's thesis, University of Bergen.

Mölders, N., S. E. Portera, C. F. Cahillb, and G. A. Grellc (2010, April). Influence of ship emissions on air quality and input of contaminants in southern alaska national parks and wilderness areas during the 2006 tourist season. *Atmospheric Environment 44*, 1400–1413.

Riddle, E. E., P. B. Voss, A. Stohl, D. Holcomb, D. Maczka, K. Washburn, and R. W. Talbot (2006). Trajectory model validation using newly developed altitude-controlled balloons during the International Consortium for Atmospheric Research on Transport and Transformations 2004 campaign. *Journal of Geophysical Research 111*.

Shindell et al. (2008). A multi-model assessment of pollution transport to the arctic. *Atmospheric Chemistry and Physics 8*, 5353–5372.

Stohl, A. (2006). Characteristics of atmospheric transport into the arctic troposphere. *Journal of Geophysical Research 111*.

Stohl, A., H. Sodemann, A. Frank, P. Seibert, and G. Wotawa (2010). *The Lagrangian particle dispersion model FLEXPART version 8.2*.

Stohl et al. (2007). Arctic smoke-record high air pollution levels in the european arctic due to agricultural fires in the Eastern Europe in spring 2006. *Atmospheric Chemistry and Physics 7*, 511–534.

Store norske leksikon (2010). Luftforurensning: virkninger: virkninger på materialer. Nestaas,Ivar and Redaksjonen. `http://www.snl.no/luftforurensning#menuitem8`. Read 20.09.2010.

Svalbard Science Forum (2010, September). Controlled meteorological balloons successfully launched from ny-Ålesund (afg2009-439). `http://www.ssf.npolar.no/pages/news390.htm`. Read 18.11.2010.

Vogelezang, D. H. P. and A. A. M. Holtslag (1996). Evaluation and model impacts of alternative boundary-layer height formulations. *Boundary-Layer Meteorologi 81*, 245–269.

Voss, P., R. Zaveri, F. Flocke, H. Mao, T. Hartley, P. DeAmicis, I. Deonandan, G. Contreras-Jiménez, O. Martínez-Antonio, M. Figueroa Estrada, D. Greenberg, T. Campos, A. Weinheimer, D. Knapp, D. Montzka, J. Crounse, P. Wennberg, E. Apel, S. Madronich, and B. de Foy (2010). Long-range pollution transport during the MILAGRO-2006 campaign: a case study of a major Mexico City outflow event using free-floating altitude-controlled balloons. *Atmospheric Chemistry and Physics 10*, 7137–7159.

Voss, P. B., L. R. Hole, A. Mentzoni, E. Helbling, and H. Johnston (2011). Controllable meteorological balloons for arctic research. Conference abstract to the American Institute of Aeronautics and Astronautics for a presentation in September.

Warneke et al. (2010). An important contribution to springtime arctic aerosol from biomass burning in russia. *Geophysical Research Letters 37*.

World Meteorological Organization (2010). *Manual on Codes: International Codes*. World Meteorological Organization. Volume 1.2, Part B.